PULSED THREE DIMENSIONAL THZ IMAGING

A THESIS SUBMITTED TO
THE GRADUATE SCHOOL OF NATURAL AND APPLIED SCIENCES
OF
MIDDLE EAST TECHNICAL UNIVERSITY

BY

BURCU KARAGÖZ

IN PARTIAL FULFILLMENT OF THE REQUIREMENTS
FOR
THE DEGREE OF MASTER OF SCIENCE
IN
PHYSICS

JANUARY 2016

Approval of the thesis:

PULSED THREE DIMENSIONAL THZ IMAGING

submitted by **BURCU KARAGÖZ** in partial fulfillment of the requirements for the degree of **Master of Science in Physics Department, Middle East Technical University** by,

Prof. Dr. Gülbin Dural Ünver
Dean, Graduate School of **Natural and Applied Sciences**

Prof. Dr. Mehmet T. Zeyrek
Head of Department, **Physics**

Assoc. Prof. Dr. Hakan Altan
Supervisor, **Physics Dept., METU**

Examining Committee Members:

Assoc. Prof. Dr. Kıvanç Kamburoğlu
Dentomaxillofacial Radiology Dept., Faculty of Dentistry, Ankara Uni.

Assoc. Prof. Dr. Hakan Altan
Physics Dept., METU

Assoc. Prof. Dr. Alpan Bek
Physics Dept., METU

Assoc. Prof. Dr. Serhat Çakır
Physics Dept., METU

Assoc. Prof. Dr. Burak Yedierler
Physics Dept., METU

Date: January 28th, 2016

I hereby declare that all information in this document has been obtained and presented in accordance with academic rules and ethical conduct. I also declare that, as required by these rules and conduct, I have fully cited and referenced all material and results that are not original to this work.

Name, Last Name: BURCU KARAGÖZ

Signature:

ABSTRACT

PULSED THREE DIMENSIONAL THZ IMAGING

Karagöz, Burcu

M.S., Department of Physics

Supervisor: Assoc. Prof. Dr. Hakan Altan

January 2016, 75 pages

In this thesis, a Terahertz Pulsed Imaging (TPI) system based on Terahertz Time Domain Spectroscopy (THz-TDS) was constructed to non-destructively evaluate and image samples. By scanning samples in the time domain, three dimensional (3D) views of sample geometries were generated. In order to image samples in 3D, a THz-TDS system based on reflection mode which permits the scanning of samples across THz beam was constructed. Thus, third axis which characterizes the depth profile of samples was obtained. THz pulse was focused on samples with an angle of incidence of 34° to a measured spot diameter of 3 mm. In the system, InGaAs based photoconductive antennas (PCAs) were used for THz generation and detection and a bandwidth up to 1 THz was obtained. Terahertz images of two different types of samples were presented to examine the constructed THz imaging system. The first sample was composed of acetate layers and letters cut from aluminium foil which were placed at various cross sections in depth. The second sample type was tooth slices of thickness ~ 1 mm sectioned mesiodistally in parallel. These tooth samples were prepared by the Faculty of Dentistry of Ankara University in Ankara, Turkey. By using this system, 3D images of the layered sample could be extracted by performing a time domain analysis although THz images were obtained from raw

THz data. It has also been shown that THz imaging can be used to detect and monitor dental caries.

Keywords: Terahertz Pulsed Imaging, Terahertz Time Domain Spectroscopy, Three Dimensional Imaging, Reflection Mode, Dental Caries

ÖZ

DARBELİ ÜÇ BOYUTLU THZ GÖRÜNTÜLEME

Karagöz, Burcu

Yüksek Lisans, Fizik Bölümü

Tez Yöneticisi: Doç. Dr. Hakan Altan

Ocak 2016, 75 sayfa

Bu tezde, Zamana Dayalı Terahertz Spektroskopisine (THz-TDS) dayalı Terahertz Darbeli Görüntüleme (TPI) sistemi örnekleri yıkıcı olmadan incelemek ve görüntü elde etmek için kurulmuştur. Zaman alanında örnekleri tarayarak, örneklerin üç boyutlu (3D) görüntüleri elde edilmiştir. Örnekleri üç boyutlu görüntülemek için, örneklerin THz sinyali boyunca taranmasına olanak sağlayan yansıma yöntemine dayalı bir THz-TDS sistemi kurulmuştur. Bu sayede, örneklerin derinlik profilini belirleyen üçüncü eksen elde edilmiştir. THz atımı 3 mm olarak ölçülen spot çapı ile örneklere 34° lik bir açı ile odaklanmıştır. Sistemde, THz üretmek ve tespit etmek için InGaAs tabanlı fotoiletken antenler (PCAs) kullanılmıştır ve 1 THz' e kadar bant genişliği elde edilmiştir. Kurulan THz görüntüleme sistemini incelemek için iki farklı türde örneğin THz görüntüleri sunulmaktadır. İlk örnek asetat katmanları ve örneğin derinlemesine farklı kesitlerine yerleştirilmiş alüminyum levhadan kesilen harflerden oluşmaktadır. İkinci örnek türü yaklaşık 1 mm kalınlığa sahip paralel mesiodistal yönde kesitlenmiş diş dilimleridir. Bu diş örnekleri, Ankara, Türkiye' de bulunan Ankara Üniversitesi Diş Hekimliği Fakültesi tarafından hazırlanmıştır. Bu sistemi kullanarak, THz görüntüleri işlenmemiş THz verilerinden elde edilmesine rağmen katmanlı örneğin üç boyutlu görüntüsü zaman alanı analizi yapılarak çıkartılmıştır.

Ayrıca, THz görüntülemenin diş çürüklerini tespit etmek ve görüntülemek için kullanılabilir olduğu gösterilmiştir.

Anahtar Kelimeler: Terahertz Darbeli Görüntüleme, Zamana Dayalı Terahertz Spektroskopisi, Üç Boyutlu Görüntüleme, Yansıma Yöntemi, Diş Çürüğü

To my family

ACKNOWLEDGMENTS

I am most grateful to my supervisor Assoc. Prof. Dr. Hakan Altan for his assistance, guidance and understanding. I also appreciate his continuous patience throughout my research and study.

I would like to thank to all my colleagues in Laser, Optoelectronics and Terahertz Imaging and Spectroscopy group for their valuable friendship.

And lastly, I would like to thank to my family for their endless support and love at each stage of my life. I am indebted to them for their encouragement to complete this work.

TABLE OF CONTENTS

LIST OF FIGURES

FIGURES

LIST OF ABBREVIATIONS

CW	Continuous wave
DR	Dynamic range
EM	Electromagnetic
EO	Electro optical
Er	Erbium
Fs	Femtosecond
FTIR	Fourier transform infrared
FWHM	Full width at half maximum
GaP	Gallium phosphide
GaSe	Gallium selenide
He-Ne	Helium neon
HDPE	High density polyethylene
HRFZ-Si	Hyperhemispherical undoped high resistivity float zone silicon
Hrs	Hours
Hz	Hertz
InP	Indium phosphide
IR	Infrared
$LiNbO_3$	Lithium niobate
LT-GaAs	Low temperature grown gallium arsenide

PCA	Photoconducting antenna
Ps	Picosecond
PTFE	Polytetrafluoroethylene
RD-SOS	Radiation damages silicon on sapphire
SC	Semiconductor
SI	International system of units
SI-GaAs	Semiinsulating gallium arsenide
SNR	Signal to noise ratio
TES	Terahertz emission spectroscopy
THz	Terahertz
THz-TDS	Terahertz time domain spectroscopy
3D	Three dimensional
TMR	Transverse microradiography
TPI	Terahertz pulsed imaging
2D	Two dimensional
TPX	Polymethylpentene
TRTS	Time-resolved terahertz spectroscopy
ZnTe	Zinc telluride
XMT	X-ray microtomography

CHAPTER 1

INTRODUCTION

The prefix tera- in the International System of Units (SI) indicates the multiplication by a factor of 10^{12}. Thus, 1 terahertz (THz) is equal to a frequency of 10^{12} hertz (Hz) which corresponds to the oscillation of electric and magnetic fields one trillion times per second. In vacuum, 1 THz is equivalent to

- a period: $\tau = 1/f = 1$ ps,
- a wavelength: $\lambda = c/f = 300$ μm,
- a wavenumber: $\bar{k} = 1/\lambda = 33.3$ cm^{-1},
- a photon energy: $E = hf = 4.1$ meV and
- a temperature: $T = hf/k_B = 47.6$ K

where f is the frequency, c is the speed of light in vacuum, h is the Planck constant and k_B is the Boltzmann constant [1].

THz radiation occupies a region between the infrared (IR) and microwaves bands in the electromagnetic (EM) spectrum (Figure 1.1). The frequency range of this band is accepted to be from 0.1 THz to 10 THz [2].
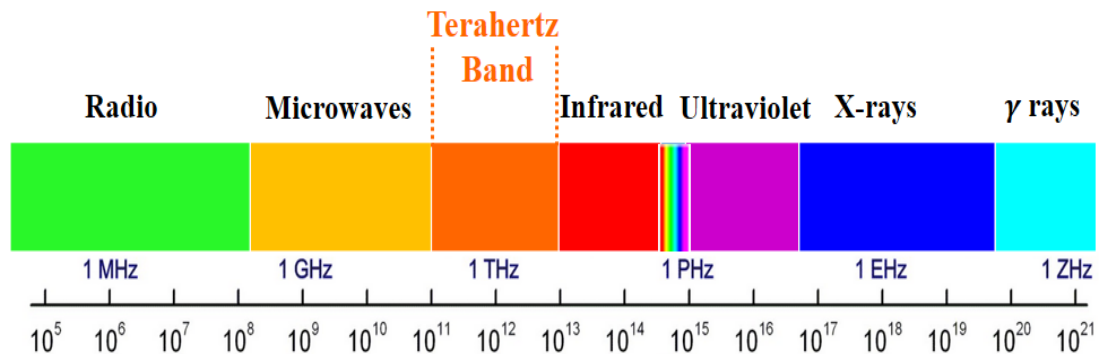
Figure 1.1: Terahertz wave region in the electromagnetic spectrum [3]

In the EM spectrum, THz waves usually designate the spectral range between the frequency bands of electronics and optics. The approaches used for electromagnetic waves below the centimeter and above the IR regions which are respectively electronics and optics (photonics) differ in terms of theoretical and technical frameworks [4]. In the millimeter and sub-millimeter waves portions, these bands experience some physical limitations [5]. Because of its specific location between the upper and lower limits of these two bands, most of the THz region has not been explored and there have been a lack of efficient generation and detection methods to emit controllable THz signals and receive information. Therefore, this part of the electromagnetic spectrum is called the "THz gap".

Despite the limited science and technology compared to the neighboring spectral bands, there has been an increasing interest in THz radiation due to its unique features [4]. The rotational and vibrational transitions of many molecules show strong absorption and dispersion at THz frequencies [6]. The location and amplitude of these resonances which are specific to molecules provide spectroscopic identification in this range. Besides this, the longer wavelengths of THz radiation compared to visible and IR waves prevent high scattering and THz waves can easily penetrate into many dry materials such as plastic, paper, textile and wood which are opaque at optical wavelengths. Likewise, an enhanced contrast can also be obtained in THz imaging methods through low scattering. On the other hand, the high absorbance of water in THz frequencies limits the penetration of THz waves into water-containing materials. Therefore, THz radiation can not present any harm to biological tissues [7] due to its limited penetration to skin. In the same way, the low photon energy of THz waves can not cause photoionization in living tissues, energy of that wave is insufficient to remove an electron. Furthermore, THz waves provide higher spatial resolution in the sub-millimeter level compared to microwaves due to their short wavelengths and enable more detailed THz images.

There are various methods to generate and detect THz waves. THz sources are generally categorized into two groups according to operating frequency and emission mode such as the continuous wave (CW) and the pulsed (time domain) sources [8]. CW systems have typically been developed from the electrical side of the

electromagnetic spectrum by the up-conversion of frequency, whereas most of the pulsed systems have been developed from the optical side. Pulsed systems rely on the generation and detection of the electromagnetic transitions using ultrafast femtosecond (fs) lasers. CW systems are tend to be narrowband and they provide continuous emission at a single frequency. Contrary to CW systems, pulsed systems are broadband sources and emission is not continuous.

THz spectroscopy and imaging are two main applications of THz wave technologies. In time domain systems, short pulses composed of many frequencies with a few picosecond (ps) duration are generated and detected. Therefore, pulsed systems are ideal in these applications because they provide picosecond resolution [9]. When the source is a pulsed laser, the commonly used spectroscopy technique is THz time domain spectroscopy (THz-TDS) [10] and the imaging technique is THz pulsed imaging (TPI).

1.1 TERAHERTZ TIME DOMAIN SPECTROSCOPY

In the far-infrared region, the spectroscopic applications have been progressing rapidly since the development of Fourier transform infrared (FTIR) spectroscopy technique in the 1950s [11]. However, FTIR does not measure phase changes which are used in the dielectric constant measurement of samples while THz-TDS does.

THz spectroscopy techniques are generally investigated in three forms [12]. These are THz time domain spectroscopy (THz-TDS), time-resolved THz spectroscopy (TRTS) and THz emission spectroscopy (TES).

In THz-TDS method, an ultrafast laser beam is split into two beams; a pump beam used to generate and a probe beam used to detect the THz pulses. The entire THz waveform is generally sampled by scanning the pump beam and recording the electric field amplitude of the THz pulse as a function of time. The spectroscopic information of a sample is extracted by the comparison of THz waveforms measured with and without a sample in the system through a Fourier transform.

In contrast to THz-TDS which probes the static properties of materials, TRTS is used to investigate the dynamic properties of samples. The TRTS setups are very similar to that of THz-TDS; however, the pulsed beam is divided into three beams for the generation and detection of the THz pulses and for optical photoexcitation. The photoinduced changes of samples resulting from the excitation through this third beam can be examined using this spectroscopic technique.

In TES, THz source is sample. The sample is irradiated with a pulsed beam which is often generated using an amplified laser which in turn generates THz radiation and the electric field amplitude and shape emitted from the sample are detected. This technique is used to measure dynamic events in samples.

THz-TDS, the spectroscopy method utilized in this thesis, is the most commonly employed technique in the characterization of spectral features of various materials in THz frequencies. It has certain benefits when it is compared to other spectroscopy methods. The coherent detection at a wide frequency range is one of the major advantages. THz-TDS has high temporal resolution due to its pulse duration in ps range. Time-gating method used in the sampling of THz pulses suppresses background noise and results in high signal-to-noise ratio (SNR) [6].

The base of many THz-TDS systems is fs pulses generated with mode-locked lasers [8] which have pulses with short duration, high power and periodic structure using mode-locking technique [13]. In THz-TDS, electro-optical (EO) (optical) rectification and photoconducting antennas (PCAs) are two common mechanisms to generate THz pulses [14]. EO sampling and PCAs are generally used in detection of THz pulses [14].

1.1.1 TERAHERTZ GENERATION METHODS

Electro-optical rectification, a second order non-linear effect, is based on the mixing of different frequency components of a fs laser pulse for the generation of THz pulses. Whenever fs pulses are focused on second order non-linear crystals, materials having a second order susceptibility different from zero, such as lithium niobate ($LiNbO_3$), zinc telluride (ZnTe), gallium phosphide (GaP), indium phosphide (InP)

or gallium selenide (GaSe), the polarization states of them are affected from the electric field. The susceptibility can be modeled as a power series where second and higher order terms of the polarizability are non-linearly proportional to the applied electric field. The interaction of photons at different frequencies of laser pulse creates a frequency dependent polarization. This induced polarization $\vec{P}$ can be defined as a power series of the electric field $\vec{E}$ associated with the laser pulse

$$\vec{P} = \varepsilon_0 [\chi^{(1)} \vec{E} + \chi^{(2)} \vec{E}\vec{E} + \chi^{(3)} \vec{E}\vec{E}\vec{E} + \cdots] \tag{1.1}$$

where ε_0 is the permittivity in vacuum and $\chi^{(n)}$ is the n th order susceptibility tensor. Electro-optical rectification results from the second term of Eq. (1.1) and polarization due to optical rectification is then expressed as

$$P_x^{(2)} = \sum_{y,z} \varepsilon_0 \chi_{xyz}^{(2)} E_y(\omega) E_z^*(\omega) \tag{1.2}$$

where $\chi^{(2)}$ is the second order susceptibility and x, y and z are notations indicating Cartesian coordinates.

The amplitude of THz field is directly proportional to the second order time derivative of this polarization. The electric field of the THz pulse ($\vec{E}_{THz}$) is expressed as

$$\vec{E}_{THz} \propto \frac{\partial^2 \vec{P}^{(2)}}{\partial t^2} \tag{1.3}$$

However, there is an impact of some factors such as crystal thickness, pulse duration of laser, crystal orientation, absorption, dispersion and phase matching conditions on the efficiency of radiation and bandwidth. This non-linear process typically allows a broadband THz spectrum about 30 THz [2].

THz pulses in the picosecond range can also be generated through the excitation of a biased PCA with fs laser pulses [15]. A PCA is composed of two metal electrodes deposited on a semiconductor (SC) material with a gap between the electrodes. Low-

temperature-grown gallium arsenide (LT-GaAs), radiation-damaged silicon-on-sapphire (RD-SOS), semi-insulating GaAs (SI-GaAs), indium phosphide and amorphous silicon are mostly used photoconductive materials. When the laser pulse illuminates the gap of antenna, photoinduced carriers, electrons and holes, are generated provided that the energy of laser pulse is higher than the bandgap of semiconducting material. The applied electric field supplied by a DC bias to the gap accelerates the carriers which will be recollected in the SC structure on ps or ns scale [10, 16] and then these carriers reach equilibrium. The movement of carriers in one direction resulting from the applied electric field generates photocurrent $J(t)$ described as

$$J(t) = N(t)e\mu E_b \tag{1.4}$$

where N is the density of photoinduced carriers, e is the electron charge, μ is the mobility of carriers and E_b is the biased electric field.

This current generates a THz wave whose electric field (E_{THz}) is expressed as

$$E_{THz} = \frac{1}{4\pi\varepsilon_0} \frac{A}{c^2 z} \frac{\partial J(t)}{\partial t} \tag{1.5}$$

where A is the area of illumination, c is the speed of light in vacuum and z is the penetration distance of the laser beam into the semiconducting material.

The amplitude of THz pulse is proportional to the derivative with respect to time of this current. The bandgap, carrier lifetime and mobility, antenna gap and bias field affect the performance of PCAs. Typical PCAs generate THz pulses up to 3 THz [17].

1.1.2 TERAHERTZ DETECTION METHODS

Electro-optic sampling relies on Pockels effect which is a refractive index or birefringence change depending on the electric field. In this sampling method, the THz field is measured by analyzing the changes in birefringence of the EO crystal,

which is also a second order non-linear effect that is reduced to a linear dependence on the applied electric field. GaP, GaAs, organic crystals, ZnTe and EO polymers are some of these crystals. The copropagation of a THz pulse and a fs laser beam inside the crystal makes the linearly polarized laser pulse into elliptically polarized. On the other hand, linearly polarized pulse is changed over to circularly polarized after its propagation through the crystal without THz pulse. A quarter wave plate is used to change the ellipticity of the laser beam and the perpendicular components of the elliptically polarized beam are separated into two parts through a Wollaston prism. A pair of photodiodes measures intensity difference of these pulses. The intensity values of these components are same when there is no THz pulse on the EO crystal and the detector measures no signal. However, when a THz pulse is focused on the crystal, there will be a signal proportional to the electric field of THz pulse because THz pulse changes the polarization of probe beam.

The PCA structures for emission of THz pulses can also be used for detection. However, the only difference between two arrangements is that electrodes in the structures of PCAs used for detection are connected to an ammeter instead of a power supply. If THz pulse illuminates the antenna gap, electron-hole pairs created by the probe beam are separated due to the electric field associated with THz pulse and this generates a current which is directly proportional to the applied electric field. However, if there is no illumination, the generation of any current is not possible. The performance of this type of detectors is dependent on the same factors that affect the efficiency of PCA emitters.

1.2 TERAHERTZ BEAM PATH OPTICAL DESIGN

In the electromagnetic spectrum, the specific location of the THz band presents some challenges. The longer wavelength (30 µm – 3 mm) of THz waves than the visible light (380-700 nm) introduces some optical restrictions in the design of optical elements used to control and guide the beam. The effect of diffraction becomes more critical as the wavelength increases; however, the surface quality of the reflective and refractive optics become less important [18].

As reflective optics, metal or gold coated off-axis parabolic mirrors are used typically in THz spectroscopy systems. The high conductivity of many metals in THz frequencies offers very little loss [19, 20]. Elliptical mirrors can also be used according to the required focusing point of THz beam [11]. On the other hand, the proper alignment of off-axis mirrors is difficult due to their geometries. The general form of the setups composed of off-axis mirrors is the 4f system, where f is the focal length of mirror. It consists of four parabolic mirrors; the generated THz wave is collimated by the first mirror, an achromatic focus is formed where the sample is located by the second mirror, the beam which is transmitted through the sample or reflected from it is then recollimated by the third mirror and the THz radiation is brought into focus on the detector by the forth parabolic mirror.

The alignment of refractive or transmissive optics is easier than reflective optics. However, the number of materials used as refractive optics is very limited [18] due to frequency dependent absorption which causes transmission losses. The attenuation of high frequency components of THz radiation prevents the operation of spectroscopy systems at high frequencies. This type of optics is usually in the form of lenses manufactured from materials that have low absorption in the THz band such as silicon, teflon, high-density polyethylene (HDPE) and picarin. High-resistivity silicon is the commonly preferred material for lenses as well as for beam splitters and filters due to its low loss and dispersion. The spherical and aspherical surfaces are typically used lens forms; however, other lens shapes such as hemispherical and hyperhemispherical have also been used. Spherical lenses are often used in the form of hyperhemispherical high-resistivity silicon lenses in the structures of PCAs.

1.3 THREE DIMENSIONAL IMAGING

THz wave imaging is one of the main applications of THz radiation. THz imaging systems can be established with both CW and pulsed sources. These two types of systems have specific strengths and weaknesses [21]. CW systems are simple and fast because they do not require pump-probe setups. Thus, the optics is uncomplicated [22] and the image formation is faster. However, despite its relative system and data complexity, imaging systems utilizing time domain approaches

provide more useful information. Unlike CW imaging which collects intensity data, pulsed THz systems record electric field. The information obtained using time domain approach in pulsed systems allows the extraction of a wide range of information such as the nature of samples [23, 24], absorption spectrum [25, 26] through analyses in the frequency domain and the depth profile [27]. Therefore, THz pulsed imaging technique provides three dimensional (3D) views of structures.

TPI was firstly reported by Hu and Nuss in 1995 [28]. They imaged a SC integrated circuit through transmission mode. In the following year, the water status and distribution of living leaves were monitored with same imaging mode [29]. Variations in the water distribution in time were clearly observed. Three dimensional terahertz imaging was firstly demonstrated in 1997 [30]. Terahertz pulses reflected from a conventional floppy disk were measured and multiple reflections from different interfaces in the sample were monitored. The images about the internal structure of disk were obtained using the time information of each of these reflections. This technique has been enhanced and THz computed tomography has been developed [31, 32]. In this technique, the target is rotated and back reflections from the sample are collected.

THz pulsed imaging employs THz-TDS principles with some additional characteristics for mapping the samples. This time domain imaging method is mostly based on the raster scanning of either the sample itself or the THz beam [33]. In the first case, sample placed at the focus of THz beam is raster scanned in a perpendicular plane to the THz pulse. In the other case, THz waveform is scanned for each pixel and thus optical delay is recorded as a function of time. Each of these spatial scans forms two dimensional (2D) THz images. However, 3D data sets can be obtained by scanning both the sample and the THz beam. Two axes obtained by sample scanning represent the vertical and horizontal spatial dimensions and the third axis offered by THz beam scanning describes the temporal (depth) dimension. Instead of raster scanning of a sample with a fixed detector, it is also possible to raster scan a fixed sample with a moving detector [34]. In this type of setups, the demanding point is to ensure the transition of the detector together with the probe beam and the optics. Likewise, a setup consisting of a fiber coupled generator and

detector mounted on an X-Y scanner can also be used to obtain 2D images while the samples are fix [35].

THz-TDS imaging has been performed with systems in transmission and reflection modes [36]. THz images in transmission mode are obtained by scanning the sample [28]. THz pulses generated by an emitter pass through the sample at the focus and the transmitted pulses are then measured by a detector. The recorded transmitted pulses for each pixel are used to generate a 2D image of the sample. In reflection imaging, reflected pulses from the different interfaces in a sample are collected. When a THz pulse is incident on the sample with a normal or off-normal angle of incidence, some part of this pulse reflects from the surface and the other part penetrates into it. At each interface variation, some part of the penetrating beam reflects. Because reflective surfaces locate at different depths, each pulse arrives the detector at distinct times. This time delay provides the depth information of each pixel. This method is called time-of-flight imaging. Thus, the internal structures of samples can be extracted.

THz pulsed imaging is a non-invasive and non-ionizing imaging technique. In this imaging method, the electric field rather than the intensity of the beam for each pixel is recorded. In this way, it enables both the identification of samples and the extraction of composition information. Small refractive index variations due to chemical or structural changes can also be detected [37]. Therefore, TPI has a wide range of applications in biology [38-40], pharmacy [41, 42], non-destructive evaluation [43] and security [44]. Three dimensional imaging utilizing TPI has also been proceeded [45-46].

In this thesis, we present a THz time domain imaging system that operates in reflection mode. This raster scan system enables the investigation of samples in three dimensions. In Chapter 2, a technical explanation of THz time domain systems for imaging, theory in detection modes with data analysis and a review of the commonly applied concepts to THz waveforms in three dimensional image formation are given. In Chapter 3, three dimensional imaging system that was constructed is explained in detail. In Chapter 4, the experimental results are shown. Finally, the experimental study is summarized in Chapter 5.

CHAPTER 2

TERAHERTZ TIME DOMAIN SPECTROSCOPY FOR IMAGING

THz pulsed imaging is principally based on THz time domain spectroscopy in transmission and reflection modes. This chapter reviews the main features of THz-TDS systems and the theoretical framework of detection modes with some basic descriptions about the propagation of THz radiation within samples. Sample analysis techniques are discussed in both modes. Then, three dimensional image construction based on reflection mode time domain spectroscopy measurements is introduced.

2.1 TERAHERTZ TIME DOMAIN SPECTROSCOPY SYSTEM

In time domain (pulsed) THz systems used in spectroscopy applications, THz pump-probe is the most widely utilized approach [17]. The generation and detection of a THz pulse using this method is based on five stages; beam splitting of the laser pulse, time delay between the pump and probe pulses, generation of the electromagnetic transient, merge of the electromagnetic transient with probe beam and detection of the THz pulse after its interaction with the sample. These stages are presented in Figure 2.1.

In a THz time domain system, a pulse generated by a fs laser is divided into two parts by using a polarized beam splitter. One portion of this pulse called pump beam generates electromagnetic transient which is the THz pulse and the other portion called probe beam detects the THz pulse. These pulses are obtained from same beam source, so pulse durations of them are same. However, the pump beam typically has much energy than the probe beam because the pump beam is used for the generation of THz pulse.

The response of a sample to a THz pulse is observed through time difference between the pump and probe pulses. A time delay is usually introduced in pump arm using a mechanical linear stage which is called delay line. In such a case, the pump beam travels along a path introduced by this line, so arrival time of the generation pulse changes with respect to the detection pulse to the detector if this line is set in motion. Thus, the entire form of THz waveform can be sampled as a function of time by scanning the relative delay time between the generation and detection beams.
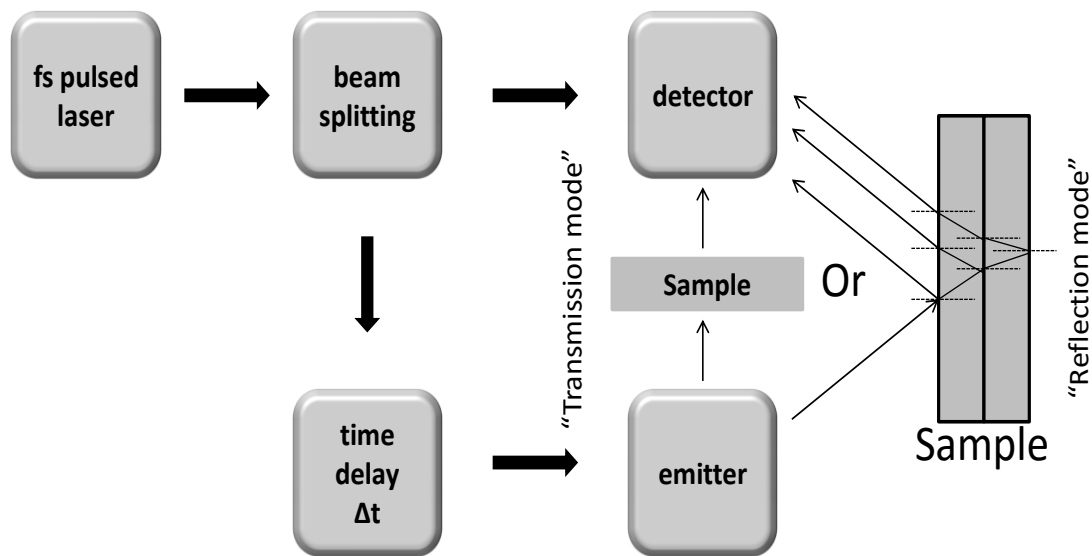
Figure 2.1: General form of THz time domain spectroscopy systems

The illumination of emitter with a pump pulse excites the SC or electro-optical material and THz pulse is generated. Pulse duration of the THz pulse is larger than the pump pulse. It is typically in the range of few ps. Then, the optically collected THz pulse is guided and focused onto the sample by lenses.

The transmitted pulses through the sample or reflected pulses as a result of normal or non-normal incidence of THz pulses on it recombine with the probe beam within the detector. A beam splitter is used in normal incidence configurations; however, this decreases the intensity magnitude of signal by a factor of 4. Non-normal incidence configurations keep away from such losses. The interaction between the pulses coming from sample and the probe beam is necessary to measure the THz pulse amplitude for specific delay times.

The amplitude of THz pulse is determined through the gate of probe beam to detector at specific time points. The detection process is the inverse of the THz generation procedure. The resulting signal is related to the convolution of the THz pulse and the probe beam that is the combination of these pulses.

In a THz-TDS setup, the most significant mechanical component is a delay unit which scans the THz pulse and provides THz waveform as a function of time. A linear stage can be positioned on the generation arm or detection arm and it is used to detect THz pulse by scanning it continuously in time. Linear stages are also used to move samples around the focus of THz beam for imaging.

In THz generation using a PCA, a bias is necessary to accelerate the photocarriers induced by pump beam. A voltage is applied to electrodes of antenna by a function generator and thus THz radiation is generated.

A lock-in amplifier is usually used to measure THz signal. An optical chopper located after the emitter or a function generator is employed to modulate the detected signal at a specific frequency. A phase sensitive detector is used in a lock-in amplifier so it operates with a reference signal. The desired signal is detected by comparing its phase and frequency with this reference. The background noise is also suppressed with lock-in amplifiers since they amplify and record the components of the detected signal which have same frequency and phase with the reference signal. Therefore, they improve signal-to-noise ratio.

2.2 TERAHERTZ TIME DOMAIN SPECTROSCOPY PRINCIPLES

In the mid- and far- infrared regions, THz-TDS and FTIR are two spectroscopic methods. While light source is THz pulses generated by a fs laser in THz-TDS, it is a thermal source in FTIR technique. They both use broadband sources, but differences between these spectroscopic techniques are explicit. FTIR can be used in a broader band than THz-TDS. Signal-to-noise of THz-TDS systems is better than FTIR for frequencies below 3 THz. However, FTIR offers better SNR over 5 THz [47].

In THz-TDS, temporal resolution is in ps scale which makes this technique suitable in time-resolved measurements. However, it is in ns scale in FTIR. The other advantage of THz-TDS is that the electric field of THz pulses is measured. Since both the amplitude and phase information are obtained through electric field measurement, absorption coefficient and complex refractive index of samples can be determined. In FTIR, intensity of light is measured and the amplitude information can only be obtained. Therefore, the Kramers-Kronig relations are necessary to extract the refractive indices of samples.

The electric field of temporally sampled THz waveform $E(t)$ can be transformed into the frequency domain via Fourier transform. The spectral distribution of electric field in frequency domain is calculated as

$$\tilde{E}(\omega) = A(\omega)e^{-i\varphi(\omega)} = \int dt\, E(t)e^{-i\omega t} \qquad (2.1)$$

where $\tilde{E}(\omega)$ is the frequency dependent complex electric field, $A(\omega)$ is the electric field amplitude in frequency domain, $\varphi(\omega)$ is the phase of electric field and ω is the angular frequency where $\omega = 2\pi f$ in which f is the frequency. Thus, the amplitude and phase information can be extracted.

Measurements either in transmission or reflection modes can be used to calculate the complex refractive index of the sample, $\tilde{n}(\omega)$. The real and imaginary components of refractive index can be shown as

$$\tilde{n}(\omega) = n(\omega) + i\kappa(\omega) \qquad (2.2)$$

where $n(\omega)$ is the real valued refractive index and $\kappa(\omega)$ is the extinction coefficient which describes the attenuation of electric field.

The complex refractive index is defined as

$$\tilde{n}^2 = \varepsilon_r \mu_r = \frac{\varepsilon}{\varepsilon_0} \frac{\mu}{\mu_0} \qquad (2.3)$$

where ε_r is the relative permittivity of the medium, μ_r is the relative permeability of the medium, ε is the medium permittivity, ε_0 is the vacuum permittivity, μ is the medium permeability and μ_0 is the vacuum permeability.

By using the assumption of $\mu = \mu_0$ for THz radiation, the complex refractive index has a form given as

$$\tilde{n} = \sqrt{\varepsilon_r} \tag{2.4}$$

The relation between the extinction coefficient $\kappa(\omega)$ and absorption coefficient $\alpha(\omega)$ is expressed by the formula

$$\kappa(\omega) = \frac{\alpha(\omega)c}{2\omega} \tag{2.5}$$

where c is the speed of light in vacuum.

The interaction of light waves with a medium can be explained through three different mechanisms which are transmission, reflection and refraction. The amplitude of electric field is attenuated during its propagation in a medium. The absorption coefficient is a fraction of this light intensity loss per unit length of the traveled distance. The attenuation is described with the Beer-Lambert law which can be written as

$$I = I_0 e^{-\alpha(\omega)d} \tag{2.6}$$

where I is the intensity at distance d and I_0 is the incident intensity.

When a wave is incident on a medium, some portion of it reflects back from the surface. The remaining portion transmits into the medium which is known as refraction (Figure 2.2). According to reflection law, the angle of reflection is equal to the angle of incidence and the relation between these angles is defined by Snell's law expressed as

$$n_i \sin\theta_i = n_r \sin\theta_r \tag{2.7}$$
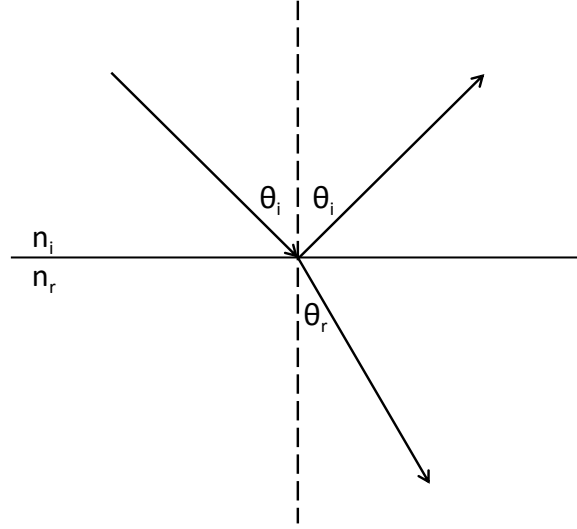
Figure 2.2: Behavior of a wave at an interface of two media having different indices of refraction where n_i and n_r are the refractive indices of medium 1 and medium 2; respectively. θ_i is the angle of incidence and reflection and θ_r is the angle of refraction.

While refraction is defined by the real valued refractive index, transmission and reflection are described with transmission and reflection coefficients of the medium, respectively. If absorption is taken into account, these quantities are replaced with complex transmission and reflection coefficients. These coefficients describe the fraction of the incident pulse which transmits through the sample and reflects from the surface and they are obtained with Fresnel's equations. In Figure 2.3, the transmitted and reflected signals during the propagation of a THz pulse through a flat layer are illustrated.

The normal incident THz pulse, $E_0(\omega)$, which includes the amplitude and phase information of the pulse is a form of incident field obtained by the Fourier transform of time domain THz pulse. If multiple reflections in the sample are ignored, the transmitted and reflected fields are then defined as

$$E_t(\omega) = E_0(\omega)t'_{12}t'_{23}e^{-\alpha d/2}e^{in\omega d/c}$$
$$E_r(\omega) = E_0(\omega)r'_{12} \tag{2.8}$$
$$E'_r(\omega) = E_0(\omega)t'_{12}r'_{23}t'_{21}e^{-\alpha d/2}e^{in\omega d/c}$$

16
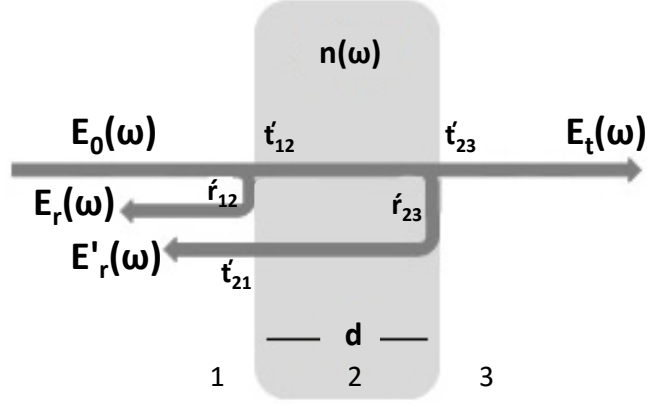
Figure 2.3: Transmission and reflection of a normal incident THz pulse passing through a single layer sample where $E_0(\omega)$ is the incident THz field, $E_r(\omega)$ and $E_r'(\omega)$ are the reflected THz fields from the entrance and exit surfaces of the sample, respectively; and $E_t(\omega)$ is the transmitted THz field. r_{12}' and r_{23}' are the complex Fresnel reflection coefficients from the first and second interfaces of the sample, respectively. t_{12}', t_{21}' and t_{23}' are the complex Fresnel transmission coefficients from region 1 to 2, region 2 to 1 and region 2 to 3; respectively. n is the refractive index and d is the thickness of the sample.

When light passes through free-space, its amplitude and phase are unchanged. However, when it passes through a sample, its amplitude is attenuated because of energy loss. Since the refractive index of the sample is higher than air, the light wave slows and the optical delay depends both on the refractive index and on the thickness of the sample.

Optical path length (OPL) through the sample is described as

$$OPL = nd \tag{2.9}$$

When light passes through a certain optical path, it undergoes a phase shift (δ). This phase change is defined in radians by the formula

$$\delta = 2\pi \frac{OPL}{\lambda} \tag{2.10}$$

where λ is the wavelength in vacuum.

17

There are also some additional phase changes due to reflection. In Figure 2.4, there is an example that shows reflections at interfaces of a layer of thickness t. Optical path length difference (Δ) of two reflected waves from this layer is given as

$$\Delta = n_2(|AB| + |BC|) - n_1|AD| \tag{2.11}$$
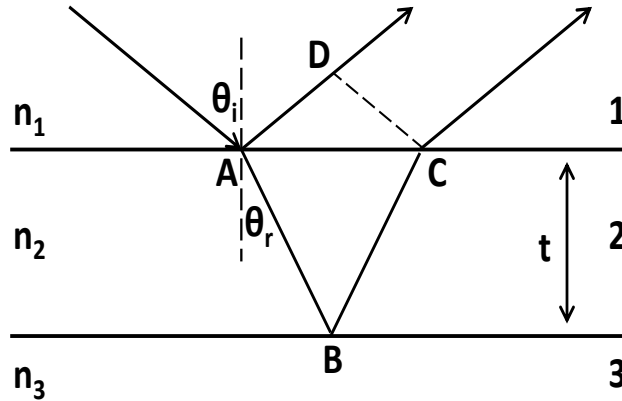
Figure 2.4: Reflections at interfaces of a layer where n_1, n_2 and n_3 are refractive indices of medium 1, medium 2 and medium 3; respectively. θ_i is the angle of incidence and θ_r is the angle of refraction.

By using Snell's law, Eq. (2.11) has a form as

$$\Delta = 2n_2 t cos\theta_r \tag{2.12}$$

The phase shift due to the path difference is then expressed as

$$\delta' = \frac{2\pi}{\lambda}(2n_2 t cos\theta_r) \tag{2.13}$$

There can be some additional phase shifts to the phase change expressed in Eq. (2.13) due to reflection. When a beam travels from a medium of refractive index n_i to a medium of refractive index n_t, the reflected beam undergoes a phase change of π radian relative to the incident beam if n_i is smaller than n_t or there is no phase change for the reflected beam if n_i is bigger than n_t.

If it is assumed that $n_1 < n_2 > n_3$ in Figure 2.4, the only phase shift is observed on reflection at point A. Therefore, the phase difference between these reflected beams can be written as

$$\delta'' = \frac{2\pi}{\lambda}(2n_2 t cos\theta_r) + \pi \tag{2.14}$$

Detection mode of a THz spectrometer is configured according to sample properties and constraints on account of its geometry. THz radiation can penetrate many materials, so the response of such samples can be measured in transmission mode. Some dry, non-polar and non-metallic matters are transparent to THz radiation, whereas some materials such as metals are opaque to THz radiation [29]. In the investigation of such non-transparent materials, THz-TDS systems operating in reflection mode are used. Dynamic range (DR) of a THz-TDS system which limits the maximum measurable absorption coefficient of a sample is frequency dependent. Therefore, highly absorbing samples can exceed the dynamic range of transmission mode systems and this prevents the determination of optical parameters. Reflection measurements can be performed when more dynamic range is required. Reflection mode is more suitable for highly absorbing, reflective and dispersive samples. Transmission spectroscopy is not appropriate samples with large thicknesses. However, reflection spectroscopy enables measurements without thickness limitation.

Transmission mode allows uncomplicated data analysis, whereas it is more difficult in reflection measurements. However, suitable methods have been improved for analyses in reflection mode. Parameter extraction principles differ in these modes. On the other hand, the response of a sample is obtained by comparing the reference and signal spectra in both modes. Reference spectrum is acquired without a sample in transmission and reflection modes and it is a single pulse. Signal spectrum is obtained by measuring transmitted pulse through the sample or reflected pulses from it and it consists of multiple pulses presenting the echoes in the sample or reflections from different interfaces of it, respectively. The analyses in the time and frequency domains after the calculation of complex transmission and reflection coefficients of samples are performed to get optical parameters of samples.

2.2.1 MEASUREMENTS IN TRANSMISSION MODE

THz time domain spectroscopy in transmission mode is usually used to determine the optical parameters of materials. The detection of both the amplitude and phase of THz waves allows to obtain optical constants without the Kramers-Kronig analysis.

A diagram showing the THz-TDS principles in transmission mode is displayed in Figure 2.5. The first signal is the reference signal obtained without a sample between the emitter and receiver. The second signal is the transmitted signal through the sample with replicas coming from internal reflections.
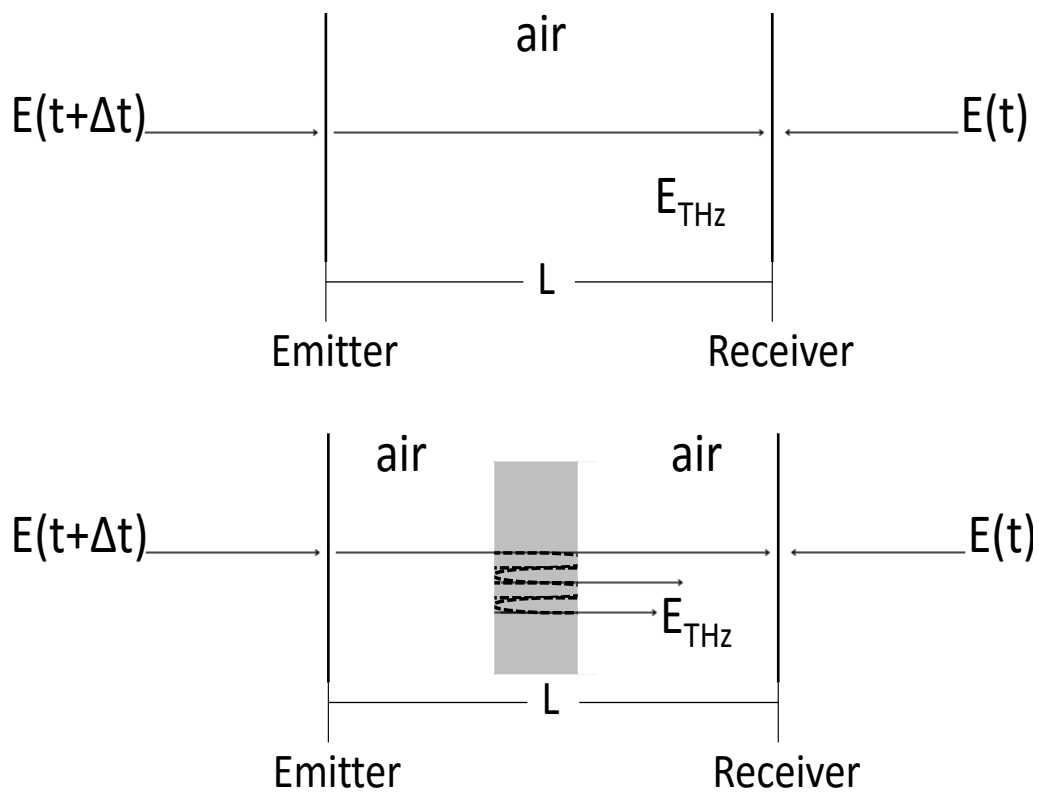

Figure 2.5: THz-TDS transmission mode measurement principles where $E(t + \Delta t)$ is the electric field of pump beam and $E(t)$ is the electric field of probe beam.

The time of flight (delay time due to optical path length) of THz pulse in a medium without a sample can be calculated as

$$t' = \frac{L}{c} \tag{2.15}$$

where t' is the elapsed time for THz propagation from emitter to receiver without sample and L is the distance between the emitter and receiver.

The time of flight of THz beam in a medium with a sample can be determined as

$$t = \frac{L - d}{c} + \frac{d}{v} \tag{2.16}$$

where t is the elapsed time for THz propagation from emitter to receiver with sample, d is the thickness of the sample and v is the speed of THz wave inside the sample where $v = c/n$ in which n is the refractive index of the sample.

The penetration time (Δt) used to determine the refractive index of the sample can be expressed as

$$\Delta t = t - t' \tag{2.17}$$

In transmission mode, the index of refraction is then found using the following formula

$$n = 1 + \frac{c.\Delta t}{d} \tag{2.18}$$

In transmission measurements, reflections are observed due to crystals used for the generation of THz pulse and boundaries of samples. These reflections appear as multiple waveforms which are replicas of the main pulse and delay of them depends both on the refractive index and on the thickness of crystals and samples. The refractive index of samples can also be calculated using the time difference between these consecutive pulses emerging from the reflection of THz pulse from sample interfaces with the following formula

$$n = \frac{c.\Delta \tau}{2d} \tag{2.19}$$

where $\Delta \tau$ is the delay time between the first and second THz pulses in the transmitted signal.

In Figure 2.6, there is a THz waveform obtained through a THz-TDS measurement of a silicon sample of thickness 200 μm. This measurement was taken using a transmission mode THz-TDS system in THz Research Laboratory, in Physics Department at Middle East Technical University (METU).
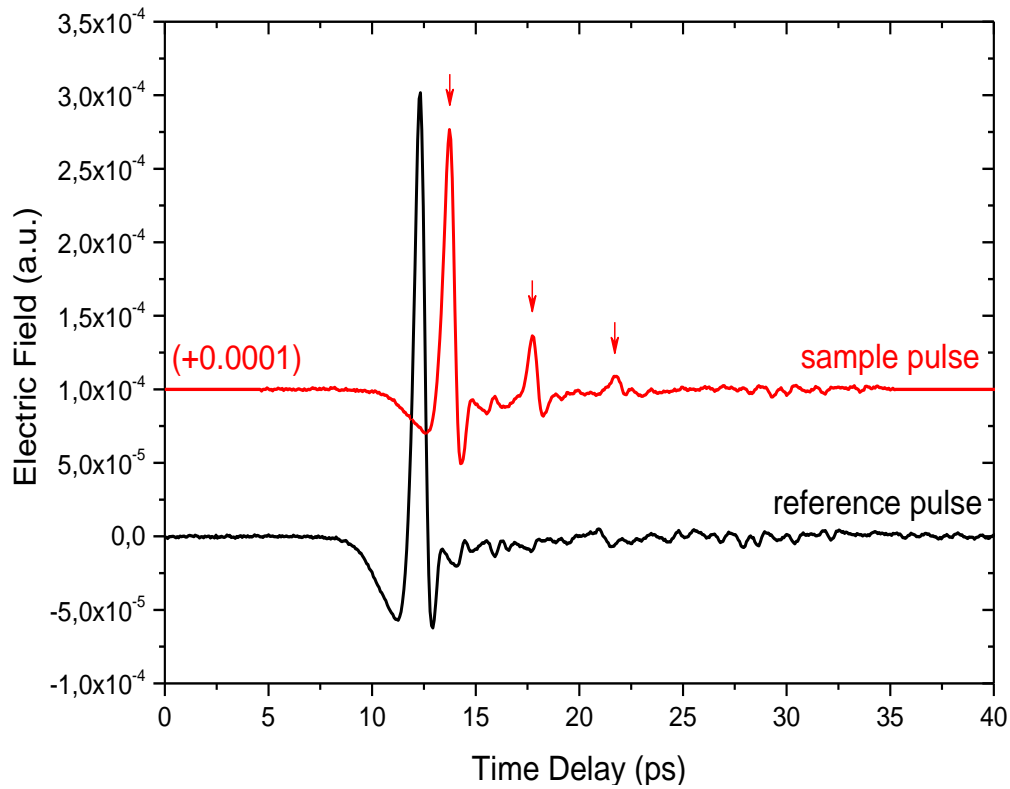
Figure 2.6: Reference and sample signals in time domain measured using a transmission mode THz-TDS system

The echoes in Figure 2.6 are well separated because silicon is optically thick; however, these will be superimposed if sample is thinner. Refractive index of the sample can be calculated by the time difference between the THz peak in air and the first THz peak in silicon because the thickness of sample is known. It can also be obtained by the time delay between the first and second THz peaks or between the second and third THz peaks in sample time domain waveform.

The amplitude and phase of THz pulses propagating through air and sample can be compared using Figure 2.3. The complex transmission coefficient $T(\omega)$ of sample is calculated as

$$T(\omega) = \frac{E_{sam,T}(\omega)}{E_{ref}(\omega)} = \tau(\omega)e^{i\phi_T(\omega)} = t'_{12}t'_{23}e^{-\alpha d/2}e^{i(n-1)\omega d/c} \qquad (2.20)$$

where $E_{sam,T}(\omega)$ and $E_{ref}(\omega)$ are the amplitudes of the transmitted and reference THz pulses, respectively. $\tau(\omega)$ is the amplitude ratio and $\phi_T(\omega)$ is the phase difference between the transmitted and reference pulses.

If the analysis is restricted to samples having low absorption coefficients, the Fresnel transmission coefficients will be real-valued and the refractive index and absorption coefficient of the sample at normal incidence are defined as

$$n(\omega) = 1 + \frac{\phi_T(\omega)c}{\omega d} = 1 + \frac{\left(\phi_{sam,T}(\omega) - \phi_{ref}(\omega)\right)c}{\omega d} \qquad (2.21)$$

$$\alpha(\omega) = -\frac{2}{d}\ln\left(\frac{(n(\omega)+1)^2}{4n(\omega)}\tau(\omega)\right) \qquad (2.22)$$

where $\phi_{sam,T}(\omega)$ and $\phi_{ref}(\omega)$ are the phases of the transmitted and reference THz pulses, respectively.

In the frequency domain, no meaningful measurements can be obtained above a specific frequency value which is called cut-off frequency. Also, this can be possible for frequencies below the cut-off because of the frequency dependent dynamic range of measurements. This is known as the strength of the reference signal according to noise floor. The highest absorbance with a dynamic range is expressed as

$$(\alpha d)_{max} = 2\ln\left(DR\frac{4n}{(n+1)^2}\right) \qquad (2.23)$$

where DR is the dynamic range.

Eqs. (2.21) and (2.22) are only valid for samples having low absorption and infinite thickness. However, additional phase shifts come from finite absorption due to complex Fresnel transmission coefficients.

In thin samples, multiple reflections occur inside the sample and these are observed as a sequence of echoes following the main pulse in the time domain signal. For such a sample, the transmission coefficient $T'(\omega)$ is the amplitude ratio of the transmitted signal $E'_{sam,T}(\omega)$ and reference THz signal given as

$$T'(\omega) = \frac{E'_{sam,T}(\omega)}{E_{ref}(\omega)} = \frac{4\tilde{n}}{(\tilde{n}+1)^2} e^{-\alpha d} e^{\frac{in\omega d}{c}} FP(\omega) \tag{2.24}$$

where $FP(\omega)$ describes the Fabry-Perot modes and is defined as

$$FP(\omega) = \frac{1}{1 - \dfrac{\tilde{n}-1}{\tilde{n}+1} e^{-\alpha d} e^{2in\omega d/c}} \tag{2.25}$$

Fabry-Perot echoes, multiple reflections in the sample, are well separated for thick samples, whereas they overlap for thin samples in the time domain expression of the transmitted pulse.

2.2.2 MEASUREMENTS IN REFLECTION MODE

THz-TDS in reflection mode can also be used to obtain spectroscopic information. In this mode, the reference signal is usually obtained by removing sample from THz focus and placing a flat metallic or dielectric mirror instead of it. These mirrors have high reflectivity at THz frequencies [48]. However, replacement of the sample can lead to some phase delay errors due to the failure in the alignment of sample position which has to be same with the reference mirror position and this can result in wrong parameter extraction [48, 49]. A window in contact with the sample can also be used for reference measurements. Reflection from the window surface is used as reference signal while the reflected signal from back surface which is in contact with the sample is the sample signal.

Determination of refractive index is one of the simplest methods to classify samples. This can be measured precisely using transmission mode THz-TDS systems [50, 51]; however, this measurement is not possible for non-transparent samples with setups in

this configuration. In the analysis of such samples, systems in reflection mode are utilized.

Many of the reflection mode THz-TDS systems have been constructed using the principle of non-normal incidence angle [52]. On the other hand, normal incidence modes in reflection mode can also be employed.

The refractive index can be calculated using the travel time information of THz pulse within the sample. The path of a THz pulse incident on a sample at a non-normal angle is shown in Figure 2.7.
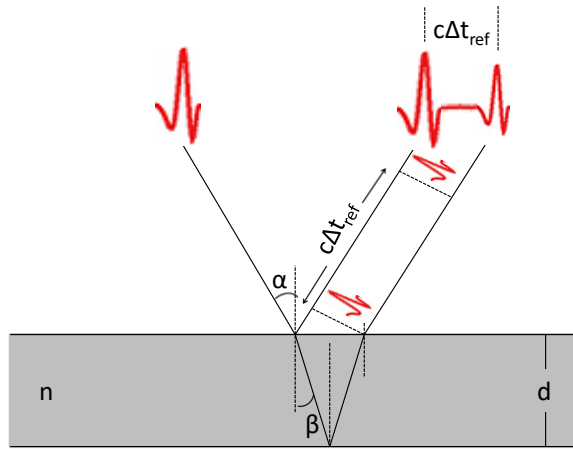
Figure 2.7: THz-TDS reflection mode measurement principles where α and β are the angles of incident and refraction, respectively. n is the refractive index of the sample, d is the sample thickness and Δt_{ref} is the time delay difference.

The geometrical path ($x_{geo,s}$) of THz pulse within the sample is calculated as

$$x_{geo,s} = \frac{2d}{cos\beta} \tag{2.26}$$

The optical path ($x_{opt,s}$) traveled is equal to the multiplication of the geometrical path with the refractive index of sample which is expressed as

$$x_{opt,s} = \frac{2nd}{cos\beta} \tag{2.27}$$

The optical path difference between the reflected pulses from the surface of the sample and from an interface inside it is then defined as

$$c\Delta t_{ref} = \frac{2d}{cos\beta}(n - sin\beta sin\alpha) \qquad (2.28)$$

By using Snell's law, $sin\alpha = nsin\beta$, Eq. (2.28) is rearranged and has a form as

$$c\Delta t_{ref} = \frac{2nd}{cos\beta}(1 - sin\beta sin\beta) = 2ndcos\beta \qquad (2.29)$$

Using Eq. (2.29), if the refractive index of the sample is known, its thickness can be calculated or if the sample thickness is known, its refractive index can be calculated without a reference measurement.

Reflected THz signal from a sample having a series of interfaces is composed of multiple pulses in sequence which have different amplitude, polarity and temporal delay. Spectroscopic parameters of the first interface are obtained by analyzing the first reflected pulse in the waveform. By combining these parameters with the second pulse, spectroscopic information of the second layer can be determined.

Refractive index of a sample can be calculated using the time difference between the adjacent reflected pulses when the THz pulse is incident on it at a normal angle as follows

$$n = \frac{c\Delta t_{normalincidence}}{2d} \qquad (2.30)$$

where $\Delta t_{normalincidence}$ is the time delay between two neighboring reflected pulses.

When a reference measurement is taken by using a metallic mirror and it is assumed that the refractive index of air is ~ 1 and the reflectivity of this mirror is high at THz frequencies, ratio of the reflected and reference THz pulses at normal incidence is given as

$$R(\omega) = \frac{E_{sam,R}(\omega)}{E_{ref}(\omega)} = r(\omega)e^{i\phi_R(\omega)} = \frac{\tilde{n}(\omega) - 1}{\tilde{n}(\omega) + 1} = \frac{n(\omega) + i\kappa(\omega) - 1}{n(\omega) + i\kappa(\omega) + 1} \qquad (2.31)$$

where $R(\omega)$ is the complex reflection coefficient of the sample, $E_{sam,R}(\omega)$ is the amplitude of the reflected THz pulse, $r(\omega)$ is the amplitude ratio and $\phi_R(\omega)$ is the phase difference between the reflected and reference pulses.

This expression involves the refractive index and absorption coefficient of the sample defined as

$$n(\omega) = \frac{1 - r(\omega)^2}{1 + r(\omega)^2 - 2r(\omega)cos\phi_R(\omega)} \qquad (2.32)$$

$$\alpha(\omega) = \frac{2\omega}{c} \frac{2r(\omega)sin\phi_R(\omega)}{1 + r(\omega)^2 - 2r(\omega)cos\phi_R(\omega)} \qquad (2.33)$$

Complex reflection coefficients $\tilde{R}_p(\omega)$ and $\tilde{R}_s(\omega)$ where subscripts p and s denote respectively parallel and perpendicular polarized non-normal incidence THz beam include refractive index and absorption coefficient information of the medium. The complex reflectivities for two polarization states through the Fresnel formulas are expressed as

$$\tilde{R}_p(\omega) = -\frac{\tilde{n}^2(\omega)\cos(\theta) - \sqrt{\tilde{n}^2(\omega) - sin^2(\theta)}}{\tilde{n}^2(\omega)\cos(\theta) + \sqrt{\tilde{n}^2(\omega) - sin^2(\theta)}} \qquad (2.34)$$

$$\tilde{R}_s(\omega) = -\frac{\cos(\theta) - \sqrt{\tilde{n}^2(\omega) - sin^2(\theta)}}{\cos(\theta) + \sqrt{\tilde{n}^2(\omega) - sin^2(\theta)}} \qquad (2.35)$$

where θ is the angle of incidence of THz radiation.

Measurement of the reflectivity of differently polarized THz radiation can be performed by turning both the emitter and detector antennas for 90°.

Complex reflectivities $\tilde{R}_p$ and $\tilde{R}_s$ are characterized by amplitudes R_p and R_s and phases φ_p and φ_s as $\tilde{R}_p = R_p e^{i\varphi_p}$ and $\tilde{R}_s = R_s e^{i\varphi_s}$, respectively. If the angle θ is

close to the Brewster angle $\theta_{Br} = tan^{-1}(n)$, the angle of incidence at which there is no reflected beam and the beam is perfectly transmitted through the medium, resonance lines will be more pronounced in the reflection spectrum. When the angle θ is equal to the Brewster angle θ_{Br}, amplitude values (R_p and R_s) tend to be zero and the study becomes more complicated.

2.3 THREE DIMENSIONAL IMAGE FORMATION

THz waveforms obtained using transmission or reflection mode THz-TDS systems for each pixel of sample contain a wealth of data that can be used to extract THz images. In the time domain, pulse shape and delays are basic contrast mechanisms for image construction. Also, transmittance and absorbance are two fundamental parameters obtained through a fast Fourier transform (FFT) for spectroscopic analysis of samples pixel by pixel. Additionally, combination of these parameters are also useful in the observation of variations between different structures.

Pulse amplitude and width, time delay and instantaneous electric field are commonly used time domain parameters in image formation. Frequency domain parameters include transmittance, time delay obtained from the phase component, absorbance, phase and dispersion.

There are two imaging modes in time domain systems due to their pulsed character. The first mode is spectral imaging. Since spectral information is obtained for each pixel in THz-TDS measurements performed utilizing either transmission or reflection mode, images can be constructed according to each frequency component through Fourier transformation. This method is appropriate for the identification of specific substances in a sample. The second mode is known as time-of-flight imaging. This mode is suitable for layered samples for the measurement of layer thickness. This imaging is performed using THz-TDS systems utilizing reflection mode and the structure of the sample is obtained by measuring the position and amplitude of reflected THz pulses from interfaces or defects inside it.

THz imaging based on reflection mode can be extended to three dimensional imaging by examining the temporal response of THz waveforms reflected from a

sample. When a THz pulse is incident on a sample, the resultant waveform is composed of a series of pulses reflected from different interfaces of the sample. Internal structure can be mapped by a time-of-flight analysis. At each time interval, amplitude of the THz field is measured and tomographic images are constructed by recording this amplitude value for each pixel. These tomographic images or C-scan images are two dimensional images corresponding to depth slices for different delay time values. Stacking up these cross sections provides a complete three dimensional structure of the sample.

The useful feature of time domain measurements is that this sampling technique allows one to discriminate positive and negative electric field amplitude values. Thus, phase shifts due to refractive index change along the THz wave propagation direction can be monitored from time domain signals. In image construction, image contrast can be obtained directly from the electric field amplitude or temporal intensity values can be used. Electric field $E(t)$ and its complex conjugate $E^*(t)$ are required to obtain intensity $I(t)$ because $I(t) \propto |E(t)|^2 = E(t)E^*(t)$. The Hilbert transform which is a conventional method in signal processing to compute the complex envelope for a signal is applied to obtain temporal intensity.

In mathematics, the Hilbert transform is an operator that produces a function $H(u)(t)$ by the convolution of a function $u(t)$ with $1/\pi t$ where the integral of the product of these two functions is taken after one of them is reversed and shifted. This transform returns an analytic signal from a real valued signal by the extention of the real signal into the complex plane. This analytic signal includes a real part derived from the original data and an imaginary part derived from the phase shift of original real data sequence. Therefore, the Hilbert transform of $E(t)$ gives a data sequence that has same amplitude and frequency content with the original one and contains phase information.

In Hilbert transform, the initial data sequence is Fourier-transformed into the frequency domain and the negative frequencies are vanished because the analytic signal has a one-sided Fourier transform. The data sequence is then Fourier-transformed into the time domain using inverse FFT and a complex valued representation of the original real data set is obtained. The length of the data set is

usually specified as a power of 2 and this can be achieved either by zero-padding that is adding 0 values on one side or both sides of data sequence or by truncating the data sequence to this length.

CHAPTER 3

THREE DIMENSIONAL IMAGING SYSTEM

In this chapter, a description of THz-TDS system constructed for three dimensional imaging of samples is given. The experimental setup with the excitation source, all optical components, electronic devices and mechanical stages is presented and THz beam path through the PCAs used for generation and detection of THz pulse is examined. Data collection modes and analyses are then described.

3.1 LASER SOURCE

A Toptica FFS.SYS laser is employed for optical excitation in this study. It is an ultrafast mode-locked Erbium (Er) doped fiber laser which generates pulses at a center wavelength of 1550 nm with a repetition rate of 89 MHz. It delivers 160 mW average power. The autocorrelation meaurement result of the laser is displayed in Figure 3.1. The pulse duration of the laser beam is measured as 230 fs using an intensity autocorrelation at full width at half maximum (FWHM) with a correction factor for Gaussian beam profile.

3.2 TERAHERTZ PULSED IMAGING SYSTEM

In this thesis, a THz time domain spectrometer operating in reflection mode which provides for three dimensional imaging of samples is constructed. Photoconductive antennas are used to generate and detect THz pulses. Optical delay line is positioned on the detection arm differently from the general structure of THz-TDS systems. The layout of the experimental setup is presented in Figure 3.2.
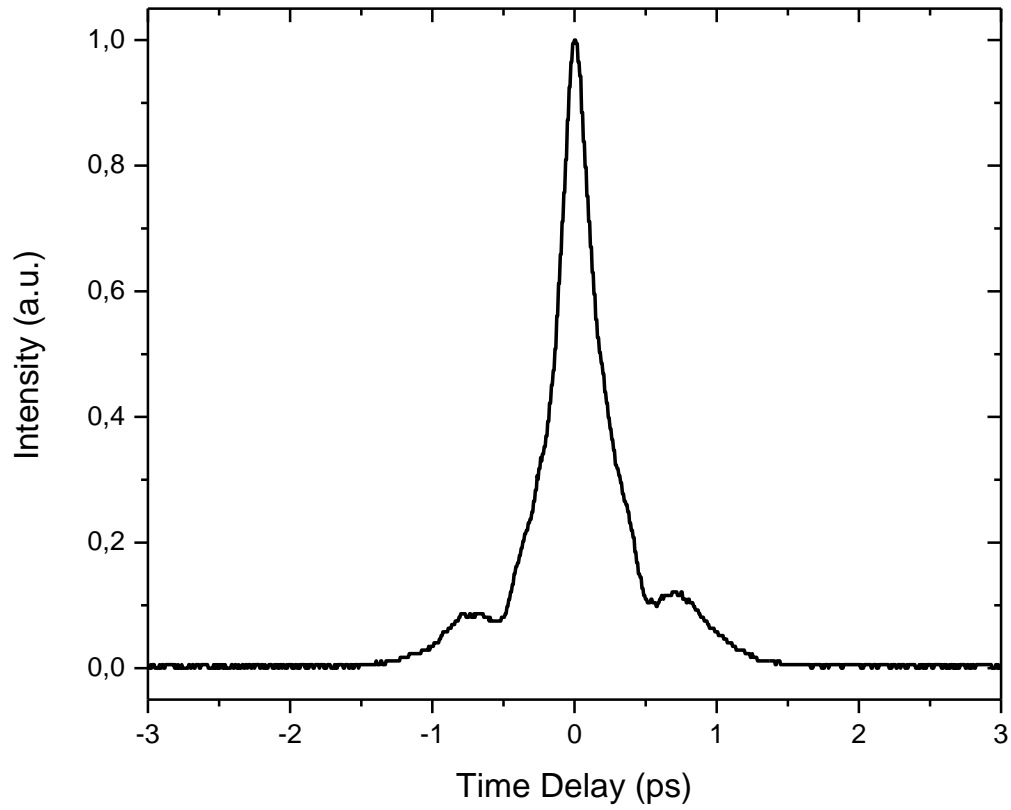
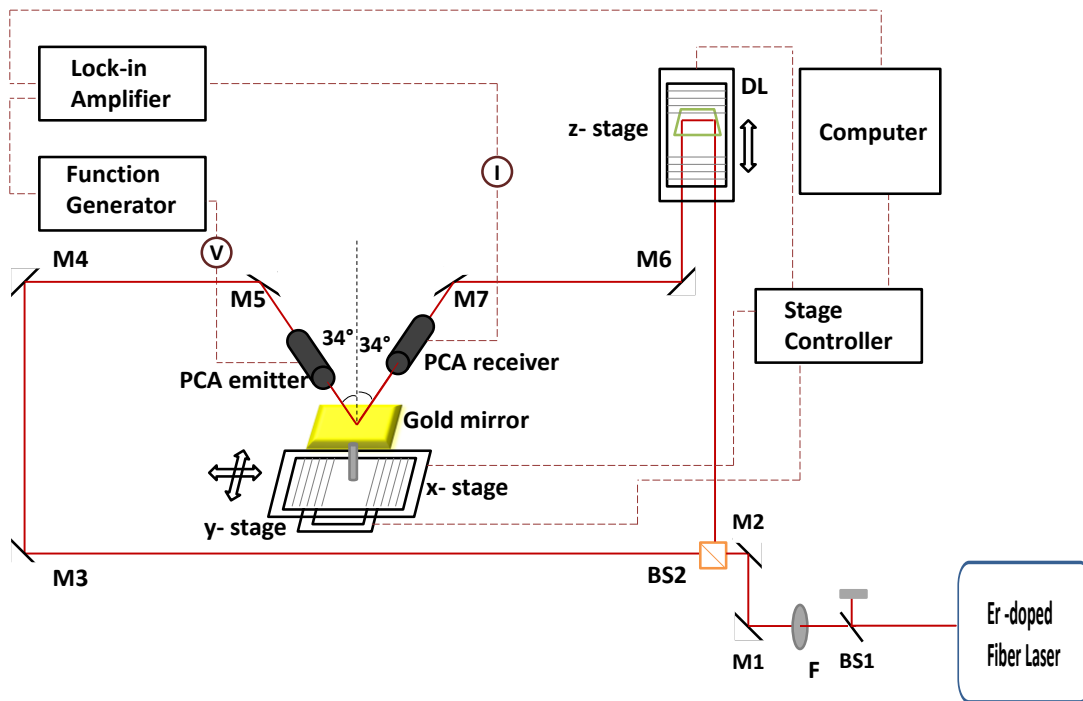Figure 3.1: Autocorrelation result of the Toptica FFS.SYS

Figure 3.2: Schematic demonstration of the experimental setup

The THz-TDS setup includes the following components which are shown in Figure 3.2:

1. Toptica FFS.SYS mode-locked Er-doped fiber laser
2. BS1: Beam splitter (Dichroic mirror)
3. F: Round continuously variable uncoated neutral density filter
4. M1, M2: Mirrors
5. BS2: Beam splitter cube (50% Transmission-50% Reflection)

    Generation arm

6. M3-M5: Mirrors
7. PCA: BATOP PCA-40-05-10-1550-h-CTL-D25mm+FTL-f30mm-l
8. Function generator: RIGOL DG2041A

    Detection arm

9. DL: Delay line with a gold corner cube retroreflector
10. M6, M7: Mirrors
11. PCA: BATOP PCA-100-05-10-1550-h-CTL-D25mm+FTL-f30mm-l

    Sample scanning and data collection

12. Gold mirror
13. x-, y- and z- stages: Newport UTS100PP
14. Stage controller: Newport ESP301
15. Lock-in amplifier: Stanford Research Systems SR850 DSP
16. Computer

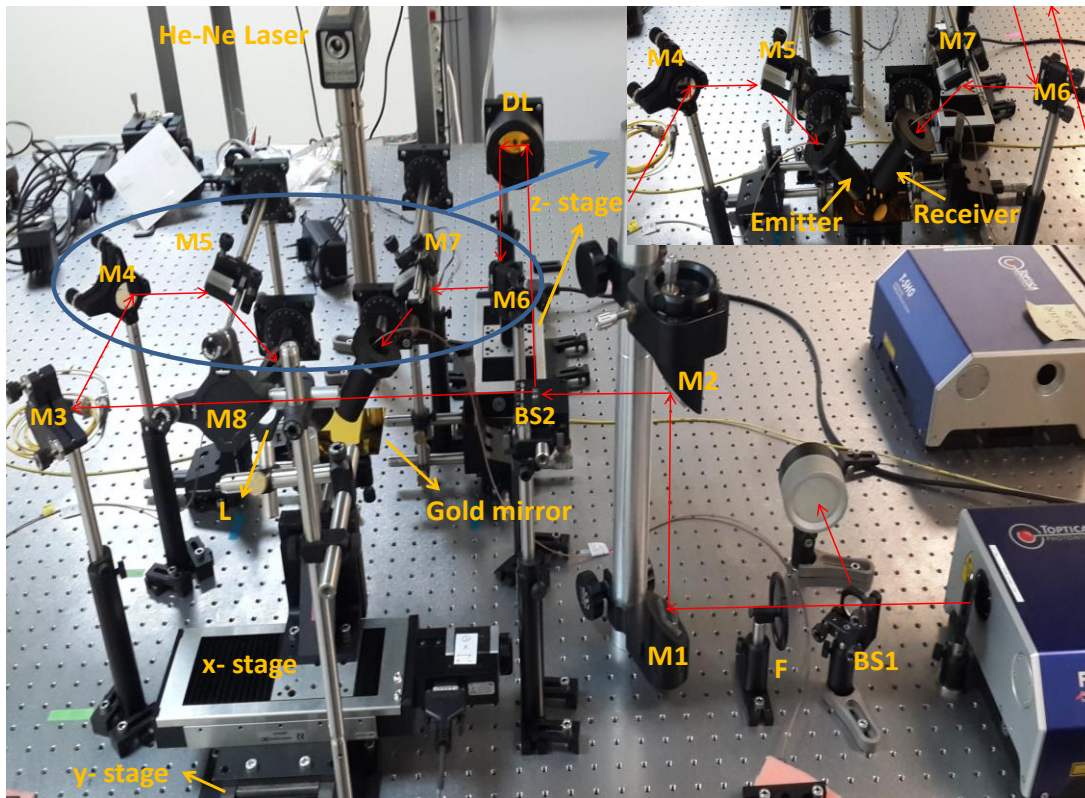The experimental setup is presented in Figure 3.3.

Figure 3.3: Labeled THz-TDS system

Components used for pointing out the position of THz beam focus which are shown in Figure 3.3:

17. JDSU Helium-Neon (He-Ne) gas laser: 0.95 mW, 632.8 nm
18. M8: Mirror
19. L: N-BK7 Plano-Convex Lens, f= 300.0 mm

Output of the ultrafast laser is divided into two parts by a beam splitter (BS1) such that a portion of the laser beam (~ 130 mW) is used in the system. A continuously variable neutral density filter (F) is placed after the beam splitter to adjust the pulse energy delivered to the PCAs. Mirrors M1 and M2 are used to rise the laser beam 30 cm from optical table surface that permits the placement of thick samples into the system. Keeping of the laser pulse at this height through the whole path is crucial because this will minimize aberration originated from other optical components.

A 50:50 beam splitter (BS2) separates the incoming beam into a pump beam that propagates through the generation arm and a probe beam that propagates through the

detection arm. Mirrors M3 and M4 are placed in the path of pump beam to make equal the optical paths of pump and probe beams. The pump beam is folded 90° by each of these mirrors and positioned to the gap of the antenna which is used for THz generation by mirror M5. This mirror is placed at angle of 62° to the normal to focus the generated THz beam on a gold mirror with an angle of incidence of 34°. The gold mirror is located at 15 cm higher than the table surface and it is used for reference measurements. Emitter is placed at an angle as the pump beam passes through its center and at a height as the focus of the THz beam is on the gold mirror. Mirror M5 and emitter are mounted to rotation stages so these angle values can be set. The power of the pump beam is measured as ~ 22 mW at a position after mirror M4.

In the setup, PCA-40-05-10-1550-h-CTL-D25mm+FTL-f30mm-l manufactured by BATOP is used to generate THz pulses. It is a parallel line antenna as emitter with LT-InGaAs semiconductor material for ~ 1550 nm optical excitation wavelength. The antenna chip size is 4 mm x 4 mm, the antenna length is 40 µm, the width is 10 µm and the gap distance is 5 µm which are shown in Figure 3.4.
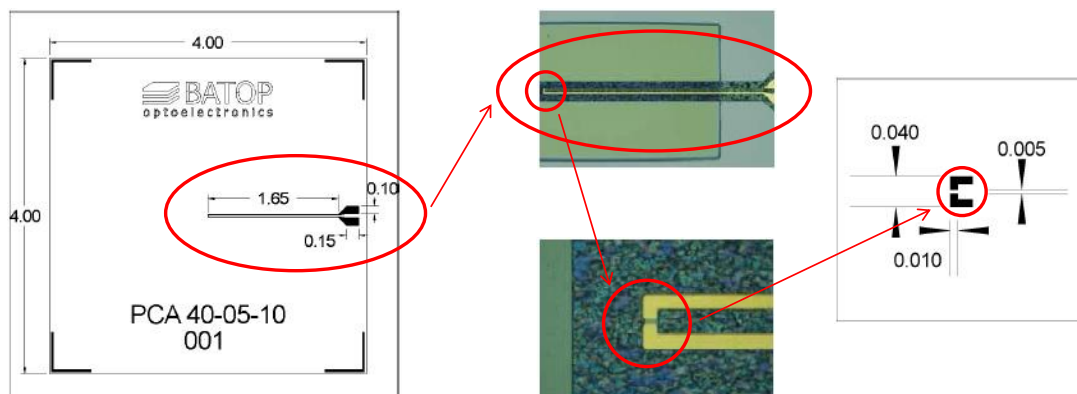

Figure 3.4: Emitter structure with dimensions (units are in millimeters) [53]

The PCA chip is mounted on an aluminium heat sink. An aspheric lens has already been placed on one side of the chip to focus the laser beam into the gap of PCA (Figure 3.5 (a)). A hyperhemispherical undoped high resistivity float zone silicon (HRFZ-Si) lens is fixed to the other side of the chip (Figure 3.5 (b)). This lens guides the THz beam through the system. These lenses on the PCA chip are shown in Figure 3.5.
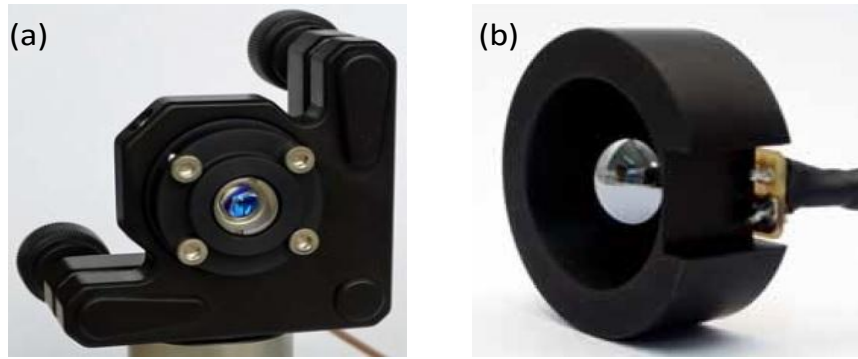
Figure 3.5: PCA chip sides with (a) an aspheric lens (b) a hyperhemispherical HRFZ-Si lens [54]

Two plano-convex polytetrafluoroethylene (PTFE, teflon) lenses have already been placed to the antenna structure to collimate THz beam and then focus it at 30 mm. A detailed explanation about the THz beam guiding in emitter structure will be given in the next section.

Focusing of the laser beam to the PCA gap is essential. Therefore, antenna attached to a rotation mount is fixed to a mirror mount. The rotation mount is used to align the antenna relative to polarization state of the pump beam and the mirror mount provides a tilt to the antenna. Then, this configuration is placed on an XYZ stage. This permits the adjustment of lateral and axial positions and height of the antenna. By altering these parameters, resistance value of the antenna is reduced to a minimum value that is an indication of maximum illumination of the antenna gap. The acquirement of the minimum resistance value indicates the start of a THz waveform measurement.

This PCA is connected to a function generator and a square wave with an output voltage of ± 5 V AC and a frequency of 1 kHz are applied to it to generate photoexcited carriers. The function generator is also connected to a lock-in amplifier so it provides a reference signal to the amplifier. Then, emitted alternating THz signal after its interaction with samples arrives to the detector.

In the detection arm, the other separated portion of the laser beam using BS2 travels towards a delay line. A retroreflector is mounted on the delay line (DL) to vary the time of the detection pulse with respect to the pump pulse and sample the THz pulse.

The alignment of the retroreflector is significant because the movement of it during the scanning process can result in a deviation of the probe beam on the detector gap. The laser beam reflects back from the retroreflector in a parallel but opposite direction and then, mirror M6 folds this beam 90° and routes to mirror M7. Combination of mirror M7 and detector is the symmetric state of the mirror M5 and emitter combination used in generation arm. The same alignments were also done for detection part to collect the reflected THz pulses. The measured power of the probe beam is ~ 23 mW at a position after mirror M6.

The reflected THz pulses from a sample are detected using PCA-100-05-10-1550-h-CTL-D25mm+FTL-f30mm-l manufactured by BATOP. A bow-tie antenna with LT-InGaAs absorber is used as a detector. The antenna chip size is 4 mm x 4 mm, the antenna length is 100 µm, the width is 10 µm and the gap distance is 5 µm which are shown in Figure 3.6.
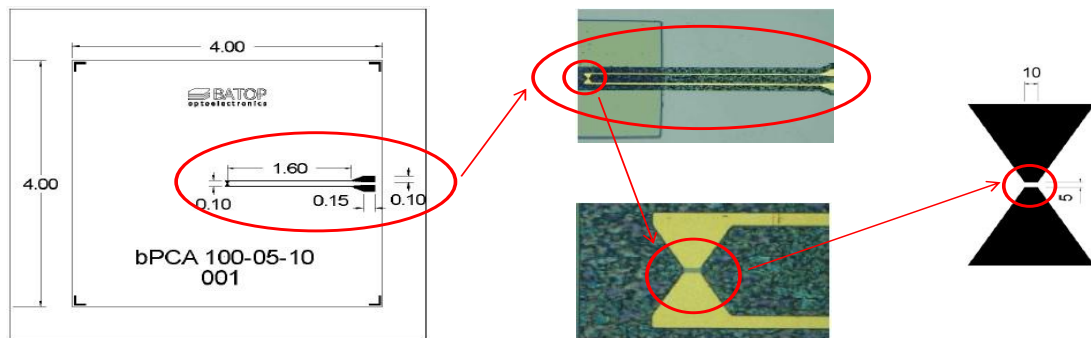

Figure 3.6: Detector structure with dimensions (units are in millimeters for antenna and in micrometers for gap) [55]

As in the emitter structure, the PCA chip is mounted on an aluminium heat sink and an aspheric lens to focus the probe beam into the gap of antenna and a HRFZ-Si lens are placed on both sides of the chip in the detector structure. Same type of teflon lenses used in emitter structure are also used in the detector.

Detector has same holder structure and it is placed on a same type of optical configuration used for the emitter. The resistance of the detector is also reduced to a minimum value. Then, the maximum THz signal amplitude is obtained by improving the adjustment of both emitter and detector using mounts and stages. Output of the

detector is an alternating current which is rectified and measured using the lock-in amplifier connected to the detector.

The x- and y- stages presented in Figure 3.2 are used to move the sample around the focus of THz beam. The gold mirror is mounted on these stages and objects to be sampled are placed on this mirror. When samples are positioned on the mirror, the height of it is aligned and the sample surfaces are set to be in THz focus. The z-stage is the delay stage and it is used to obtain THz waveforms by raster scanning. These stages provide a scanning range of 10 cm.

In the setup, a He-Ne laser is used to point out the exact position of the THz focus on the gold mirror. As shown in Figure 3.3, mirror M8 is put against this laser at an angle as the laser beam reflects from M8 and focuses on the gold mirror using a focusing lens (L) placed in front of M8. This configuration allows us to position samples in the focal point of THz beam.

3.3 THZ BEAM PATH ANALYSIS AND OPTIMIZATION

PCAs used as emitter and detector in the system are offered with a collimating teflon lens (CTL-D25) and a focusing teflon lens (FTL-f30mm). The combination of the hyperhemispherical silicon lens, collimating and focusing teflon lenses is shown in Figure 3.7.
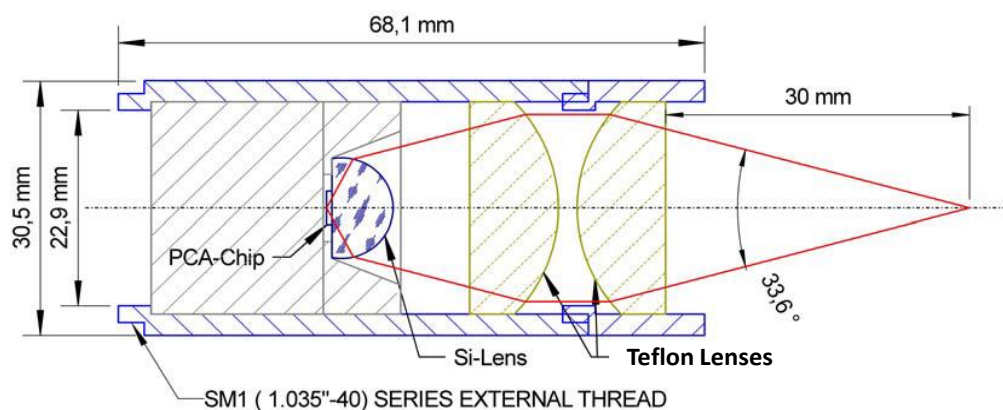

Figure 3.7: Schematic of generation and detection PCAs in combination of a hyperhemispherical silicon lens with two teflon lenses [56]

In the emitter, the hyperhemispherical silicon lens on PCA chip delivers a divergent THz beam. Therefore, it is combined with a collimating plano-convex teflon lens having a focal length of 35 mm and F#1.4. An additional focusing plano-convex teflon lens with a focal length of 30 mm and F#1.2 is mounted in front of the collimating teflon lens. THz beam focused at 30 mm in this lens arrangement.

Antennas were aligned as the THz pulse was focused on the sample with an angle of incidence of 30º in this lens configuration. However, the measured spot diameter was about 10 mm at the focus.

Focal spot size of the THz beam determines spatial resolution. A spot diameter of 10 mm offers a limited resolution for THz images. Therefore, the focusing teflon lens of emitter was replaced with a polymethylpentene (TPX) lens. It is a bi-convex F#1 lens having a focal length of 25 mm and the focal spot size is then measured as 3 mm at 18 mm. The angle of incidence is aligned to 34°. THz pulse and corresponding spectrum measured by reflection from the gold mirror after the replacement of focusing lens in the emitter structure are shown in Figure 3.8 and Figure 3.9, respectively. This THz pulse has a bandwidth up to 1 THz with a SNR of $10^4/1$.
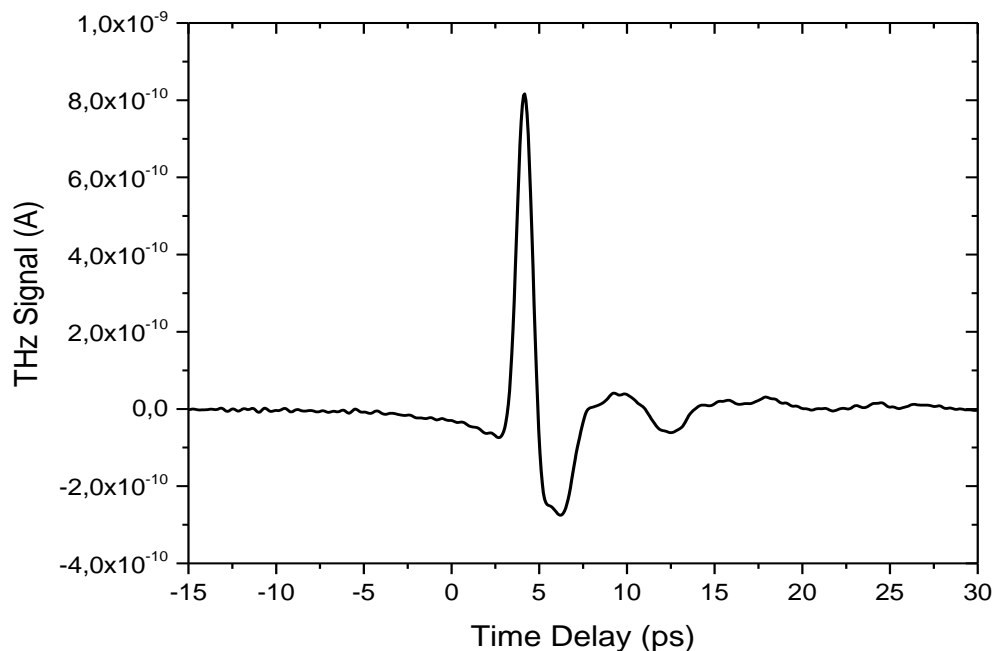

Figure 3.8: THz waveform in time domain after the replacement of focusing teflon lens with a TPX lens in emitter structure
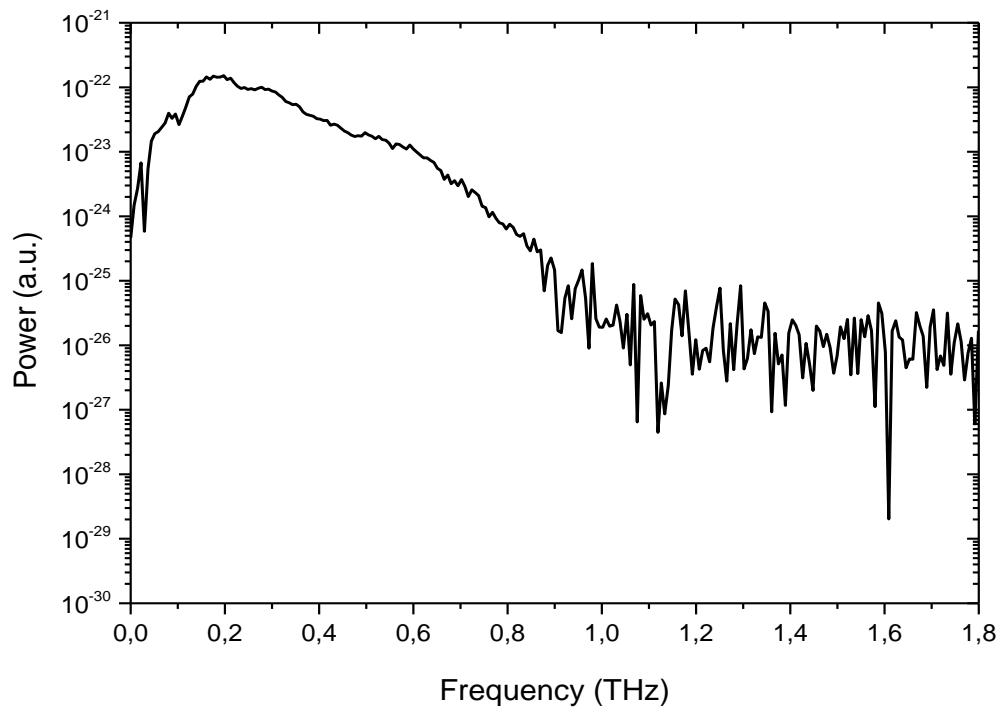
Figure 3.9: Power spectrum of the THz pulse after the replacement of focusing teflon lens with a TPX lens in emitter structure

In Figure 3.10, a visible image and a THz image of an aluminium sample with apertures of 3 mm x 3 mm in dimensions are presented. THz image of the sample shows THz peak amplitudes obtained by scanning the sample around the focal point of THz beam. The resolution of the system that is in the range of 3 mm x 3 mm can also be observed from this measurement

3.4 DATA COLLECTION AND ANALYSIS

Data acquisition is controlled by a Labview program in the system. A computer controls the stages where the communication between the computer and stages is controlled by a stage controller and collects data from the lock-in amplifier at predefined time intervals. Step size and scan distance of each translational stages and time interval between the consecutive steps are adjusted using the Labview code. Current value of the THz field is recorded from the lock-in amplifier and the entire THz waveform is mapped out in time domain.

(a)
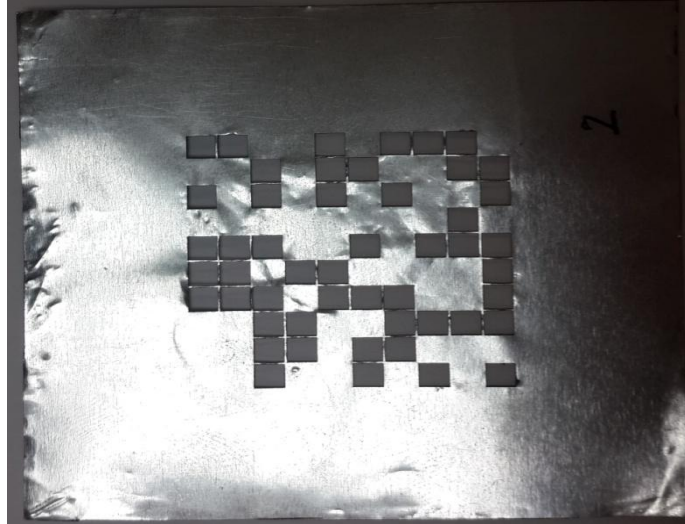
(b)
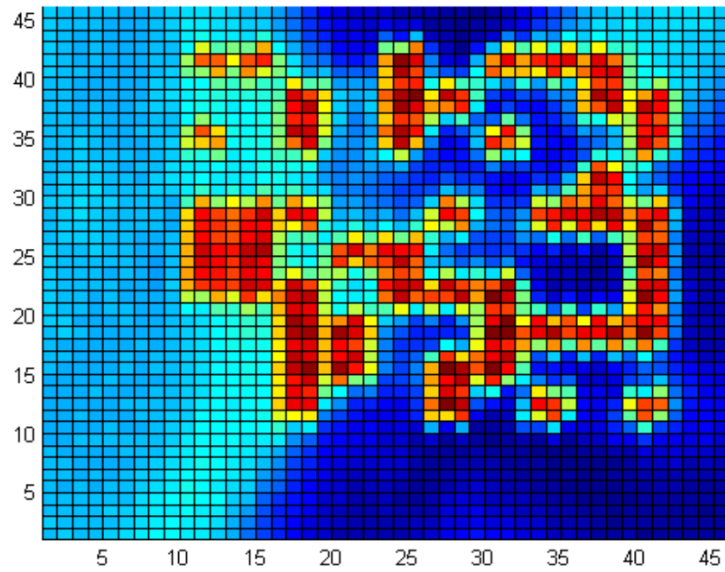
Figure 3.10: (a) Aluminium sample with apertures (b) THz false-color image of sample (scales are in millimeters); red color represents higher reflectance because of the presence of apertures.

There are two different Labview codes used in data acquisition which are for THz spectroscopy in reflection mode and for THz imaging. THz waveform is recorded for a specific point on the sample in THz spectroscopy. Delay time of the probe beam is

adjusted and THz waveform is scanned through the defined scan distance. These measurements were generally executed with 10 μm step size and 300 ms wait time between each steps. This means that stage scanning the THz waveform (z-stage) moves 10 μm, waits 300 ms and reads THz field amplitude and then repeats this procedure until it reaches its final position.

In THz imaging, THz waveforms are recorded for each pixel on the sample. Two modes of operation are possible for THz imaging. In the first mode, amplitude of the THz pulse at a specific delay time is recorded for each pixel. This provides a 2D image that shows the surface or interface variations of the sample. In the second mode, amplitude of the whole THz field is recorded for each pixel. This provides a 3D image that shows the internal structure of the sample.

In THz imaging measurements, the first step of the procedure is to define pixels. Sample is considered as a two dimensional matrix and it is then divided into portions. Each of the components of this matrix is a pixel that will create the THz image. Step size specified along the width and height of the sample together with the dimensions of the sample gives the number of pixels defined. Total number of pixels can be expressed mathematically as

$$Pixel\ number = pixel\ per\ row \times pixel\ per\ column \quad\quad (3.1)$$

$$= \frac{width\ of\ sample}{step\ size\ along\ x\ direction}$$

$$\times \frac{height\ of\ sample}{step\ size\ along\ y\ direction}$$

The next step is to scan the sample around the focus of THz beam. Image acquisition process with the created spatial matrix and direction of the motion along the pixels is presented in Figure 3.11. Motion determined in the code starts from the top leftmost pixel and moves along the row with defined steps. When data is recorded for all pixels along that row, it is moved to the next row along the last column and this procedure continues until the scan of all pixels is completed. Step size along the vertical and horizontal directions determines resolution and this size is determined according to the dimensions of details on samples.

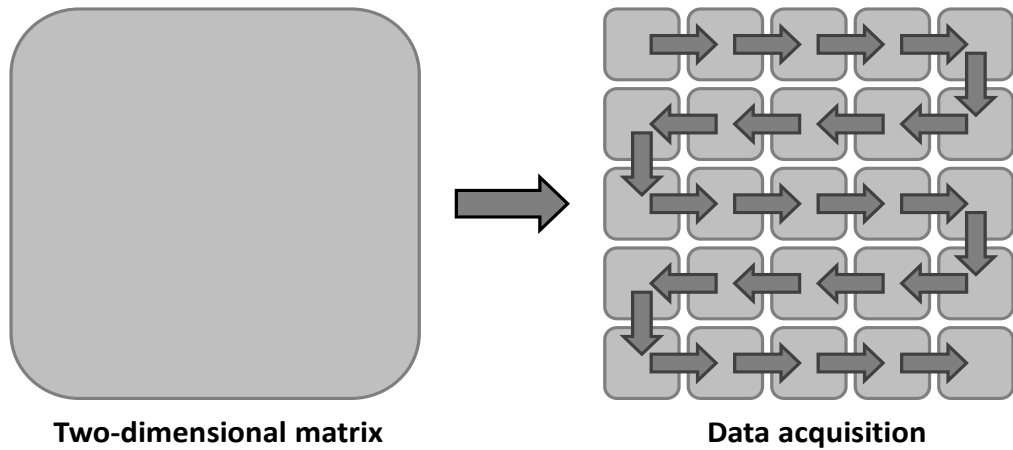**Two-dimensional matrix**   **Data acquisition**

Figure 3.11: THz imaging sample scanning procedure

In the first THz imaging mode, a single time point measurement is taken. Delay stage (z-stage) is kept at a fixed point and THz amplitude is recorded at this delay time for each pixel by moving the sample around the focus of THz beam (by x- and y-stages). Since a single quantity is measured, it is not possible to perform an analysis in frequency domain. However, data acquisition time is adequately shortened. This mode of imaging is exemplified in Figure 3.12.
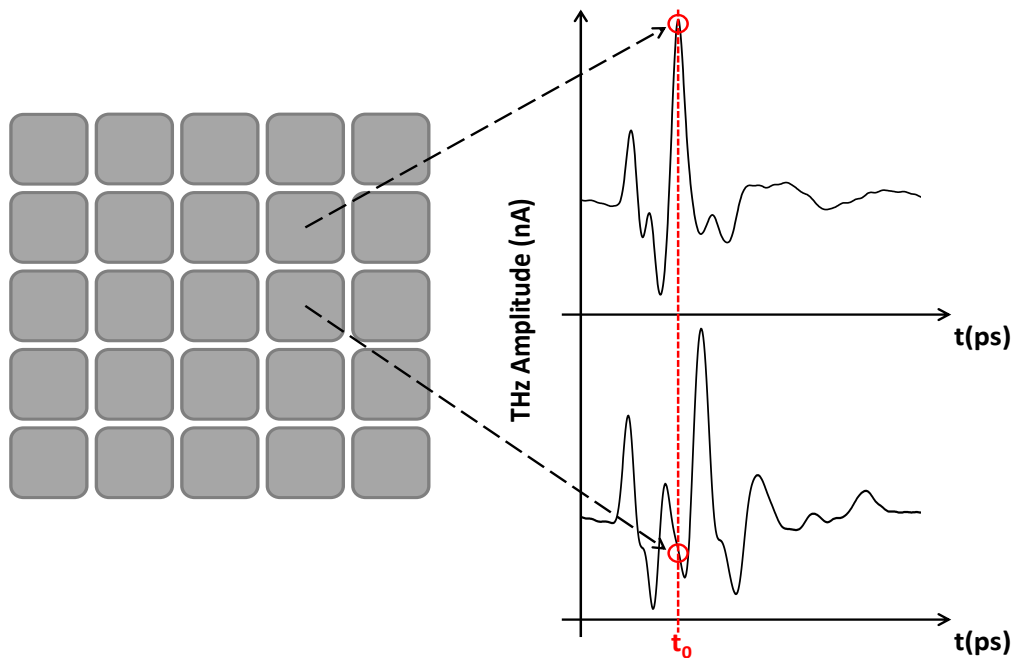

Figure 3.12: THz imaging mode based on a single point measurement in the THz waveform

In the second THz imaging mode, the entire THz waveform is measured for each pixel. Since spectroscopic information of all of the pixels is recorded, this mode allows us to extract sample properties through frequency domain analyses. Data acquisition time is considerably large because of raster scanning technique used to collect information. On the other hand, delays due to different interfaces can be observable in the THz time domain signals. Thus, it provides information about the structure of samples and 3D images of them can be formed. Length of the scanning is determined by the thickness and refractive index of the sample. This mode of imaging is illustrated in Figure 3.13.
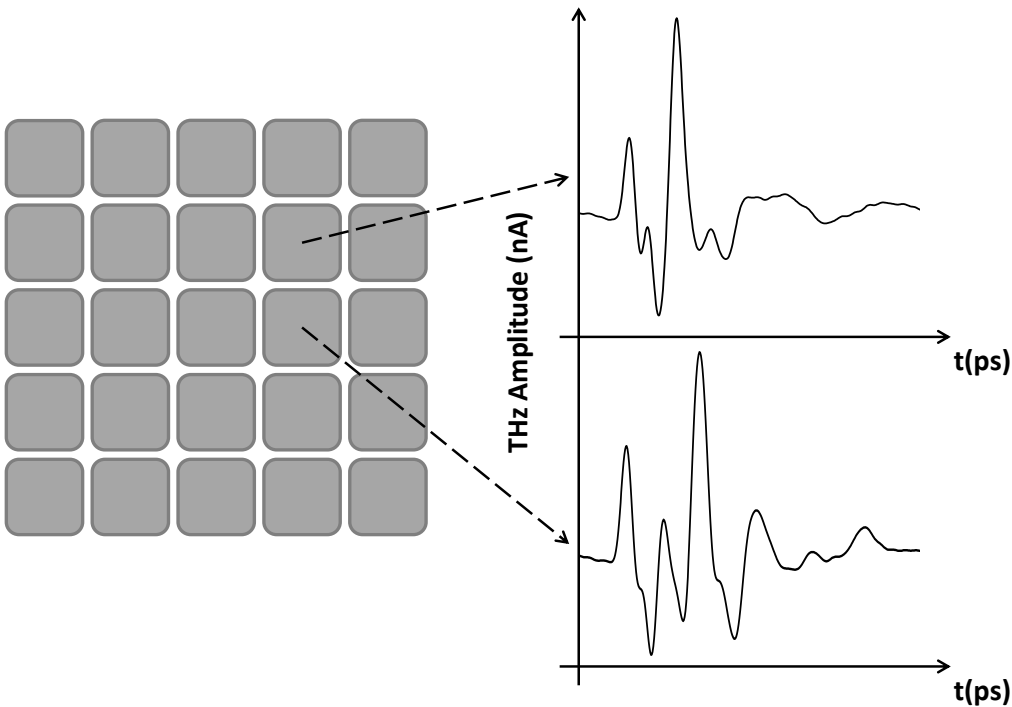
Figure 3.13: THz three dimensional imaging mode based on the entire THz waveform measurement

Data analyses are performed with some available softwares such as Origin and MATLAB in this study. Time domain and frequency domain analyses are executed depending on what is examined in samples. In the time domain analysis, image contrast is extracted using THz field amplitude or magnitude of each pixel for a fixed or different time delays. Fixed delay time analyses provide THz images which are helpful in the observation of the surface or thickness variations of samples through

arrival time change of THz pulses. Measurements taken by scanning the THz waveform for each pixel enable the extraction of three dimensional images of samples. In the frequency domain analysis, time domain signal is preprocessed by data deleting or zero-padding process applied to the original data sequence before the FFT calculations.

In this study, raw THz-TDS data obtained from measurements is used for two and three dimensional image construction. In 3D imaging, THz signals are collected from each pixel of the scanned area and they are regarded as that they describe a three dimensional structure where x- and y- axes describe two dimensions and delay axis, time axis, characterizes the third dimension. Then, combined time domain THz signals for each pixels are plotted using MATLAB.

CHAPTER 4

THREE DIMENSIONAL SAMPLE GEOMETRIES

In this thesis, a THz time domain spectroscopy system utilizing reflection mode was constructed for three dimensional imaging of samples. Experimental results are presented in this chapter. Terahertz images of two types of items were generated to examine the constructed THz imaging system presented in Chapter 3. The first part of this chapter includes an explanation about samples investigated in this study and the second part contains THz imaging results of these samples. In the last part, these studies performed to comprehend the interaction of THz radiation with certain samples and the eligibility of the constructed system to extract three dimensional profile of samples with and without different interfaces are discussed.

4.1 SAMPLES

Terahertz images of two different types of samples are presented in this study. The first sample is composed of acetate layers and three letters in different sizes and shapes cut from aluminium foil. The second type of samples is tooth slices having thicknesses of approximately 1 mm.

A sample consisting of acetate layers in which some letters made of aluminium were embedded was prepared to examine the efficiency of the system in monitoring the internal structure of a material. Thicknesses of acetate sheets were 100 µm and aluminium letters were 80 µm. Three letters having different shapes and sizes were inserted at various cross sections in depth by cutting specific regions of acetate sheets in the shape of letters and acetate papers together with aluminium letters were stacked as displayed in Figure 4.1. This sample was composed of six layers and its

total thickness was 600 μm. The letters were located to second, third and fifth layers.

Tooth samples for this study were obtained with an ethical approval from the Faculty of Dentistry of Ankara University, Ankara, Turkey. These samples were permanent tooth slices sectioned mesiodistally in parallel. In segmentation, a water-cooled diamond saw operating at low speed was used, thereby tooth sections and dental caries can be monitored. These slices were then inspected using a stereomicroscope (x10) (Stemi 2000; Carl Zeiss, Jena, Germany). Slices stored in distilled water were dried in air before the examination. Figure 4.2 demonstrates visible images of tooth slices studied in this thesis.
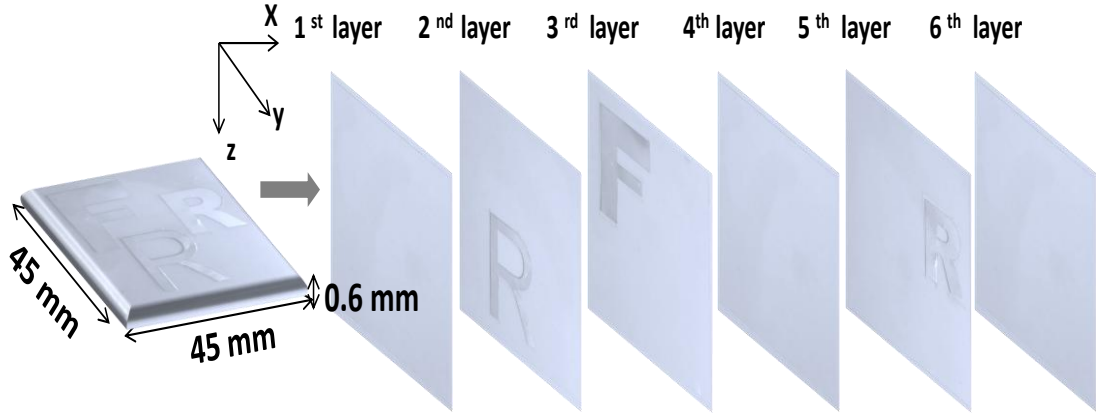

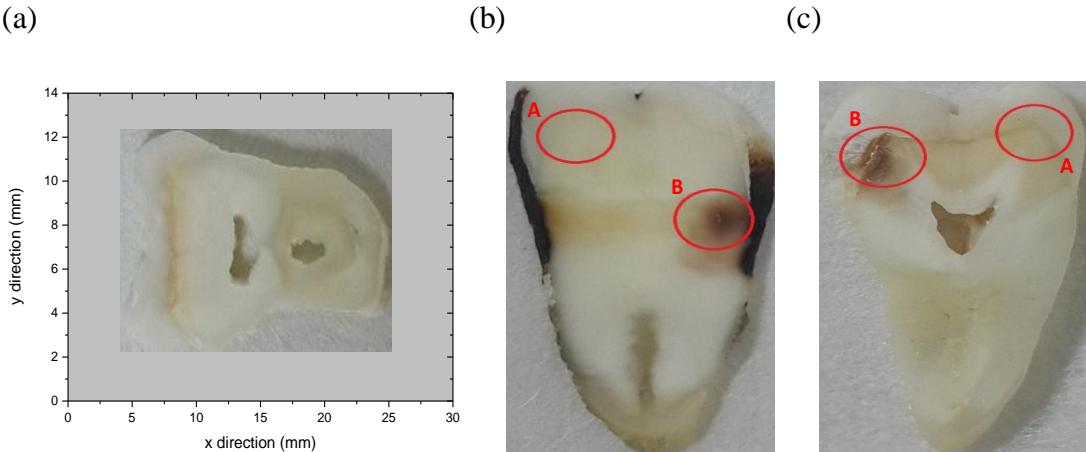Figure 4.1: Visible image of layered sample

Figure 4.2: Sliced (a) tooth sample 1 with scale (b) tooth sample 2 (c) tooth sample 3 where (A) and (B) indicate healthy and caries points, respectively.

4.2 TERAHERTZ IMAGING RESULTS

4.2.1 TERAHERTZ IMAGING RESULTS OF MULTILAYER SAMPLE

Discontinuities in refractive index through the depth of a sample result in multiple reflections. These reflections become evident in resultant THz waveforms as distinct peaks at different time delays. Because each variation inside the sample leads to a reflection, each peak in time domain signal indicates location of interfaces. By analyzing these peaks, three dimensional structure of the sample can be reconstructed.

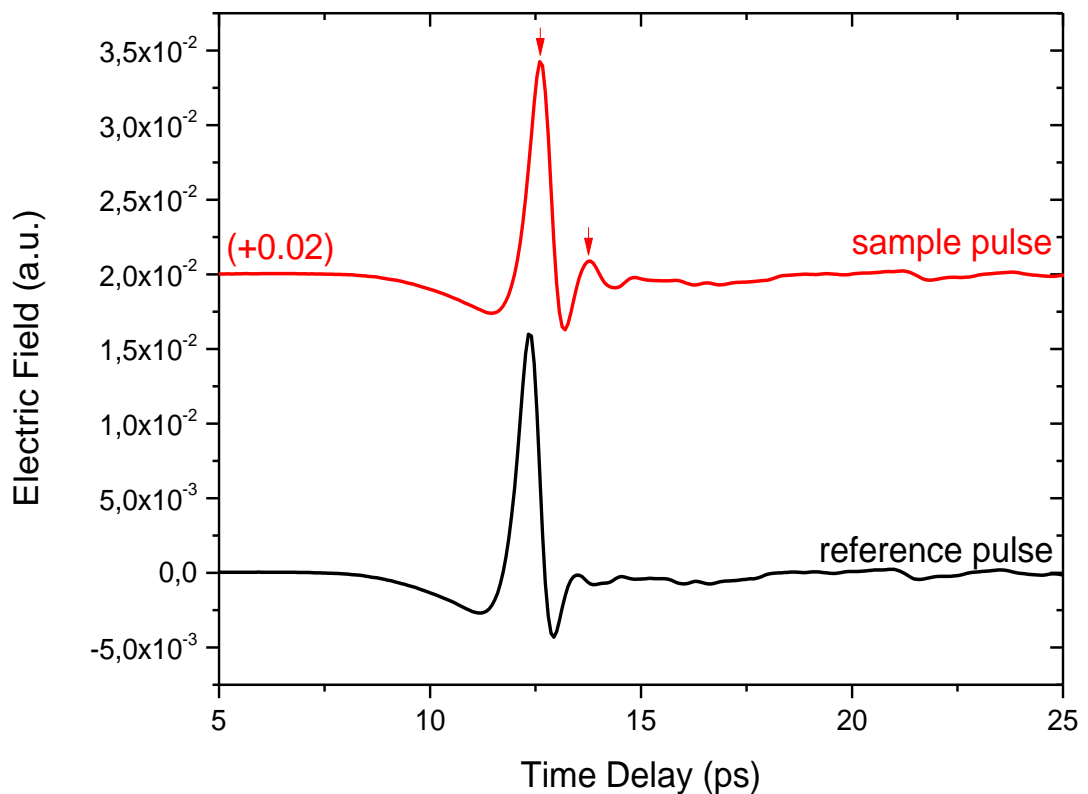Figure 4.3: Reference signal and sample signal transmitted through an acetate layer in time domain measured using a transmission mode THz-TDS system

In a detailed examination of the depth of interfaces, refractive index information of acetate is required. Figure 4.3 shows time traces of reference THz signal and transmitted THz signal through an acetate layer. Refractive index of the acetate was

calculated as 1.8 by time difference between the THz peak in air and the first THz peak in acetate using Eq. (2.18) or by time delay between the first and second THz peaks in sample spectrum using Eq. (2.19).

Time-of-flight analysis of the THz pulse provided for characterizing the examined sample. There were variations in the time of flight of THz pulse, because reflecting interfaces were located at different depths. The changes in reflected electric field for different positions in depth through the layered sample are shown in Figures 4.4 – 4.9. The normalized amplitude of electric field as a function of time was used in Figures 4.4 – 4.6 and the normalized magnitude of electric field obtained by Hilbert transform as a function of time was used in Figures 4.7 – 4.9. Each time point in the recorded THz waveforms was converted into a layer inside the sample. These images corresponded to slices of 0.06667 ps of THz waveforms and this time frame was equivalent to 0.01 mm depth resolution in air. These THz C-scan images were acquired across the 44 mm x 44 mm surface of the layered sample with a 2 mm spatial step size over the surface.

Multiple THz scans were performed in the construction of a three dimensional depth profile of the sample. Scanned area of each cross sections corresponded to 484 point measurements in which each pixel contained 280 time data points. Scanned region of the THz waveforms for each pixel was equivalent to an uncorrected 2.8 mm (18.7 ps) length in depth. Measurement of each row, 2 mm in width, defined on sample as shown in Figure 3.11 was taken separately with 200 ms wait time between each steps in z- direction and total measurement of the layered sample was completed in a period of 10 Hrs.

Time axis of each images in Figures 4.4 - 4.9 presents THz delay as a result of its propagation through the layers of the sample. THz waveforms for each pixel were aligned as that reflection from the surface of the sample occurred at 0 ps and this layer was denoted as 0 mm. These optical delays were not corrected for refractive index change; however, depth values of each layers given in C-scan images were corrected using the index of refraction of acetate. From the 0 mm image to the 0.818 mm image, they show layers into the sample. Letters cut from aluminium foil are expected to be observed at 120 µm, 220 µm and 420 µm in THz images.

Figure 4.4: Cross sectional THz images of multilayered sample in z- direction at 0 mm, 0.134 mm and 0.216 mm inside the sample (false color images of normalized electric field amplitude); the red color shows high reflectance.

Figure 4.5: Cross sectional THz images of multilayered sample in z- direction at 0.251 mm, 0.351 mm and 0.473 mm inside the sample (false color images of normalized electric field amplitude); the red color shows high reflectance.

Figure 4.6: Cross sectional THz images of multilayered sample in z- direction at 0.555 mm, 0.666 mm and 0.818 mm inside the sample (false color images of normalized electric field amplitude); the red color shows high reflectance.
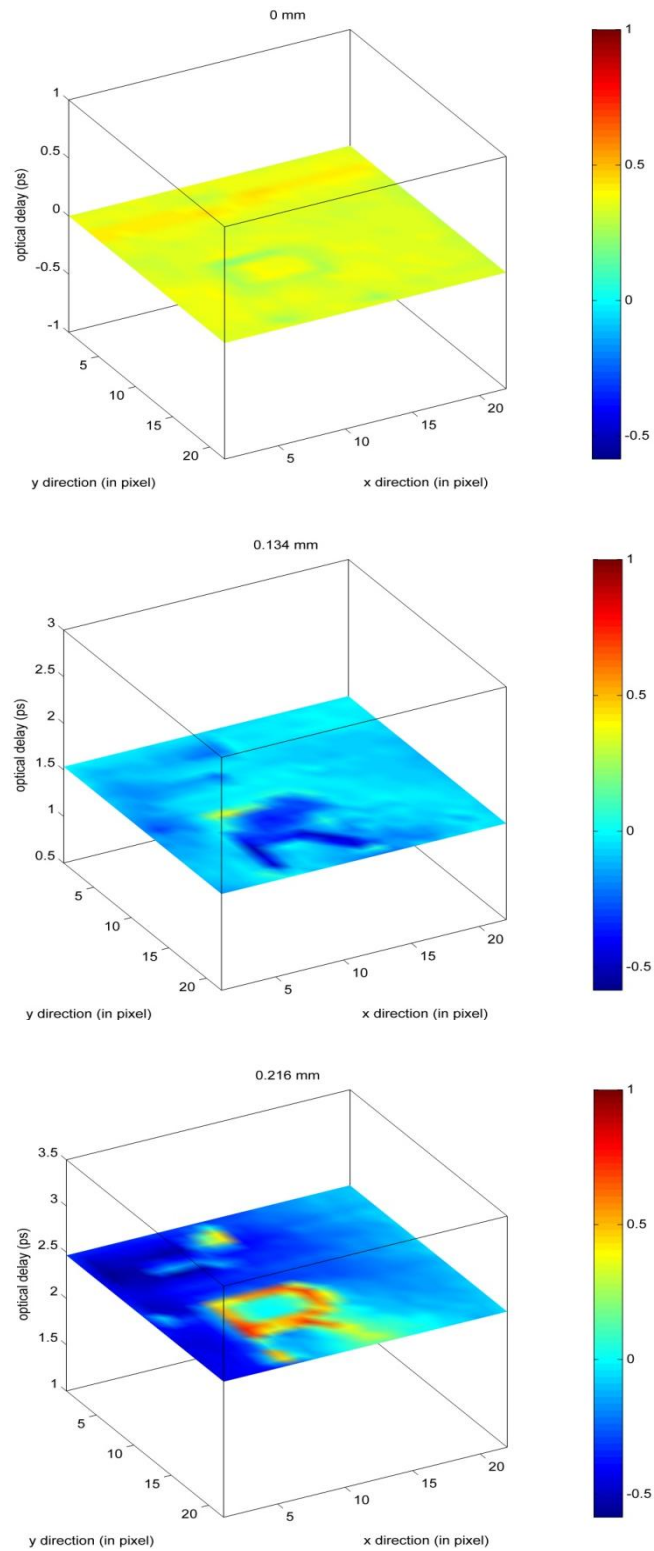
Figure 4.7: Cross sectional THz images of multilayered sample in z- direction at 0 mm, 0.123 mm and 0.216 mm inside the sample (false color images of normalized electric field magnitude); the red color shows high reflectance.
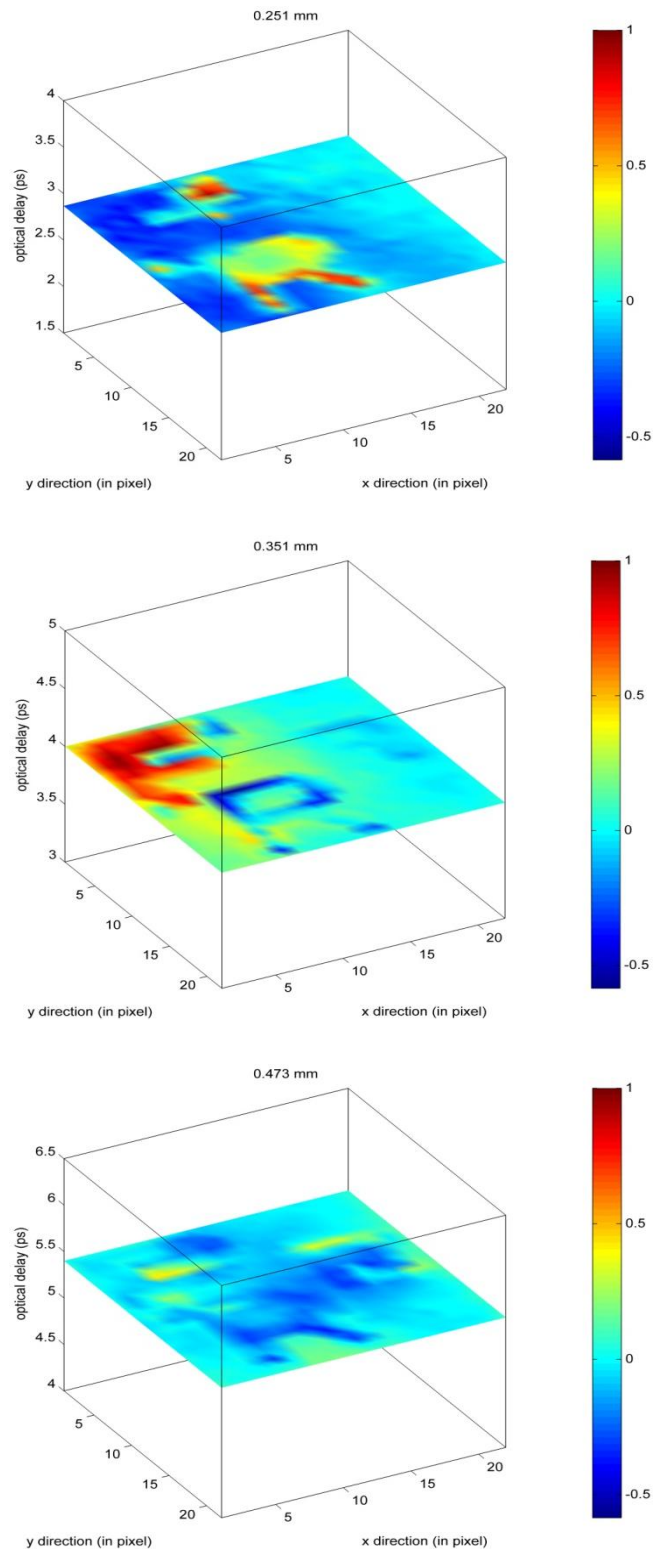
Figure 4.8: Cross sectional THz images of multilayered sample in z- direction at 0.251 mm, 0.351 mm and 0.473 mm inside the sample (false color images of normalized electric field magnitude); the red color shows high reflectance.
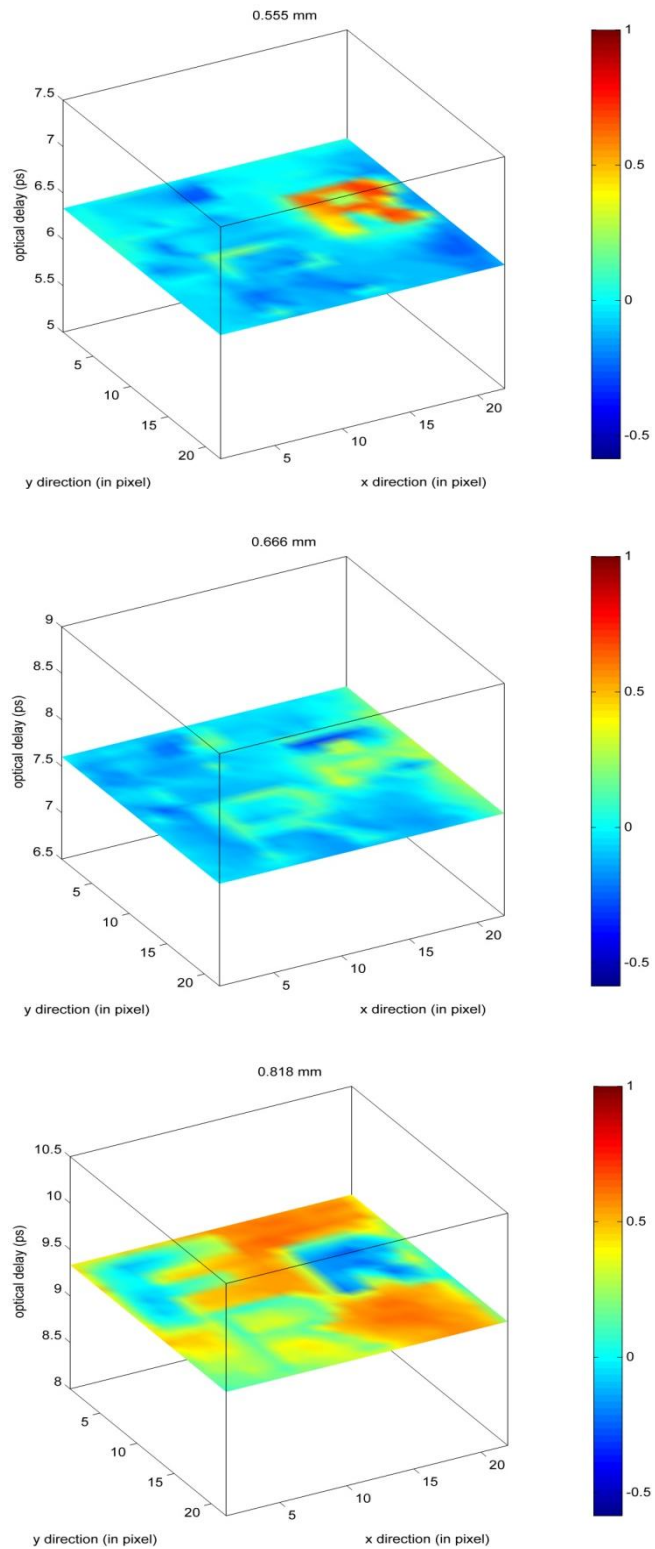
Figure 4.9: Cross sectional THz images of multilayered sample in z- direction at 0.520 mm, 0.666 mm and 0.818 mm inside the sample (false color images of normalized electric field magnitude); the red color shows high reflectance.
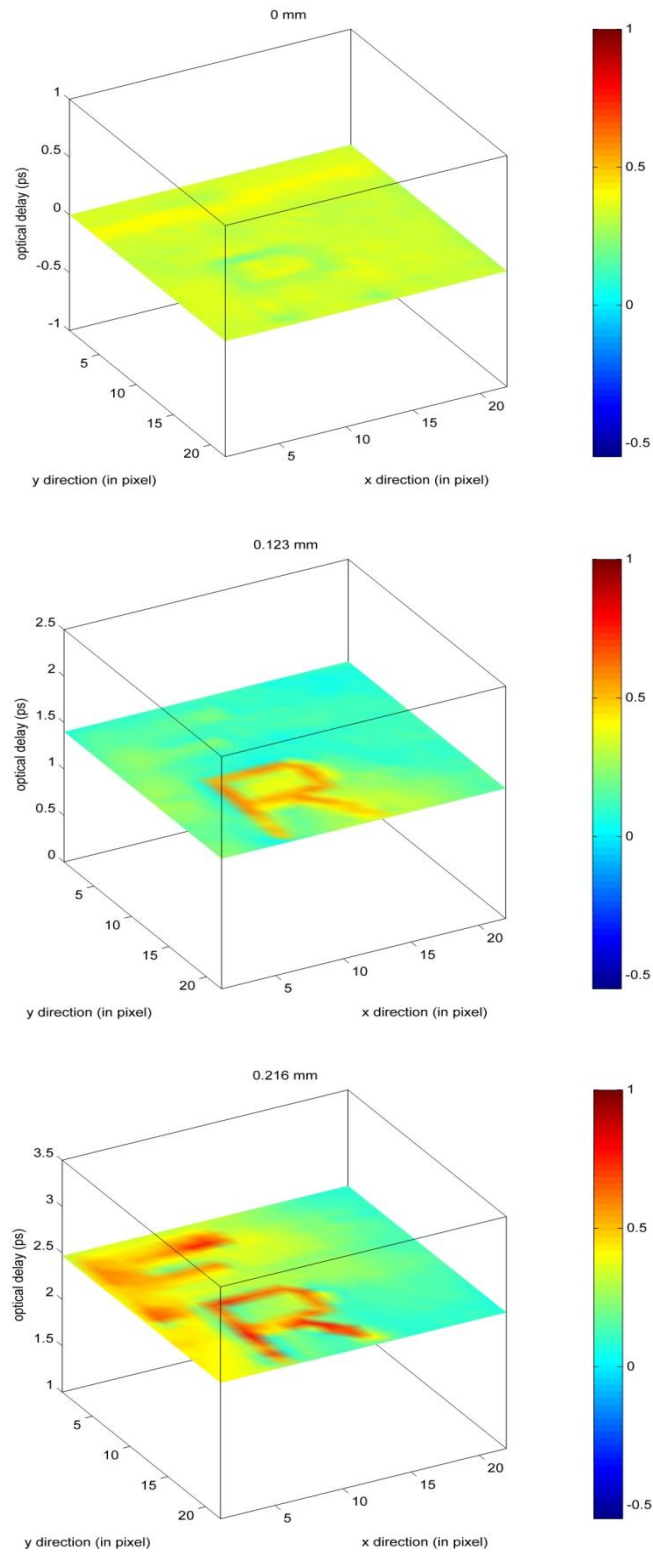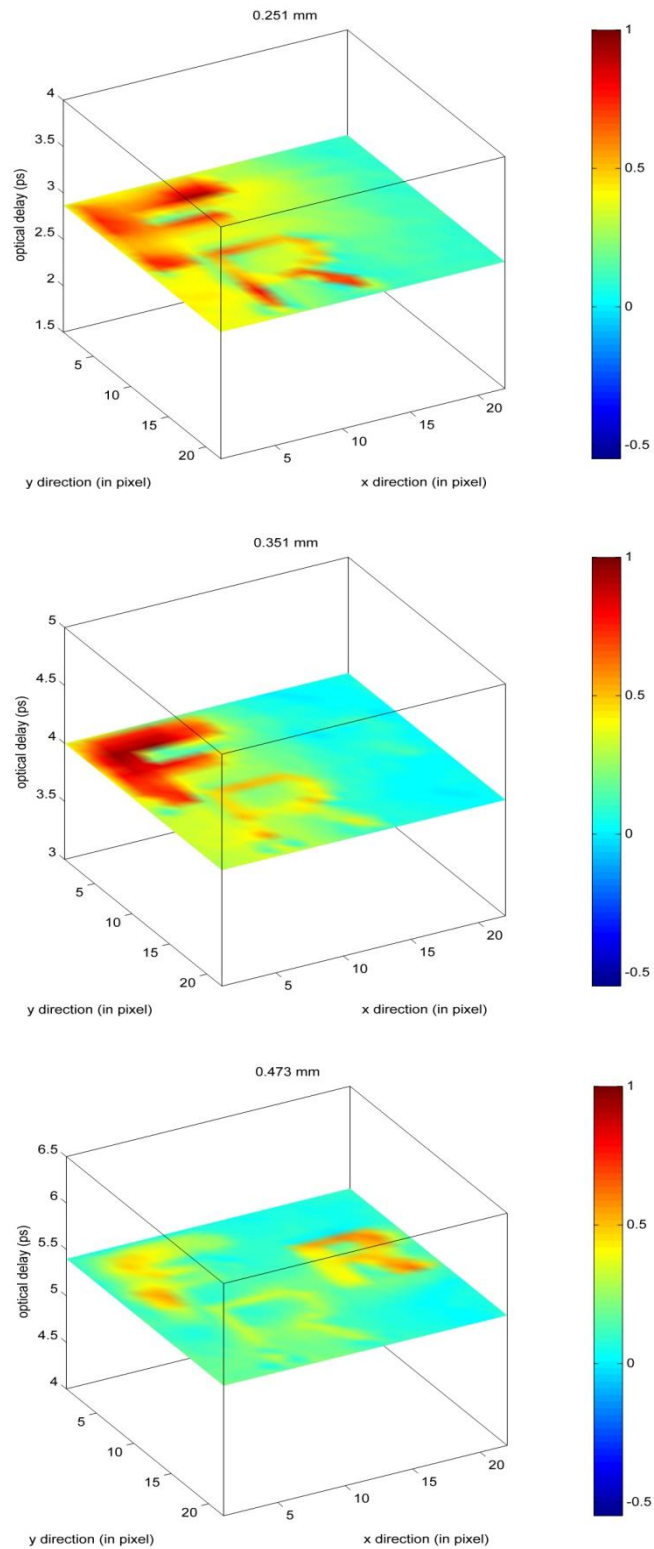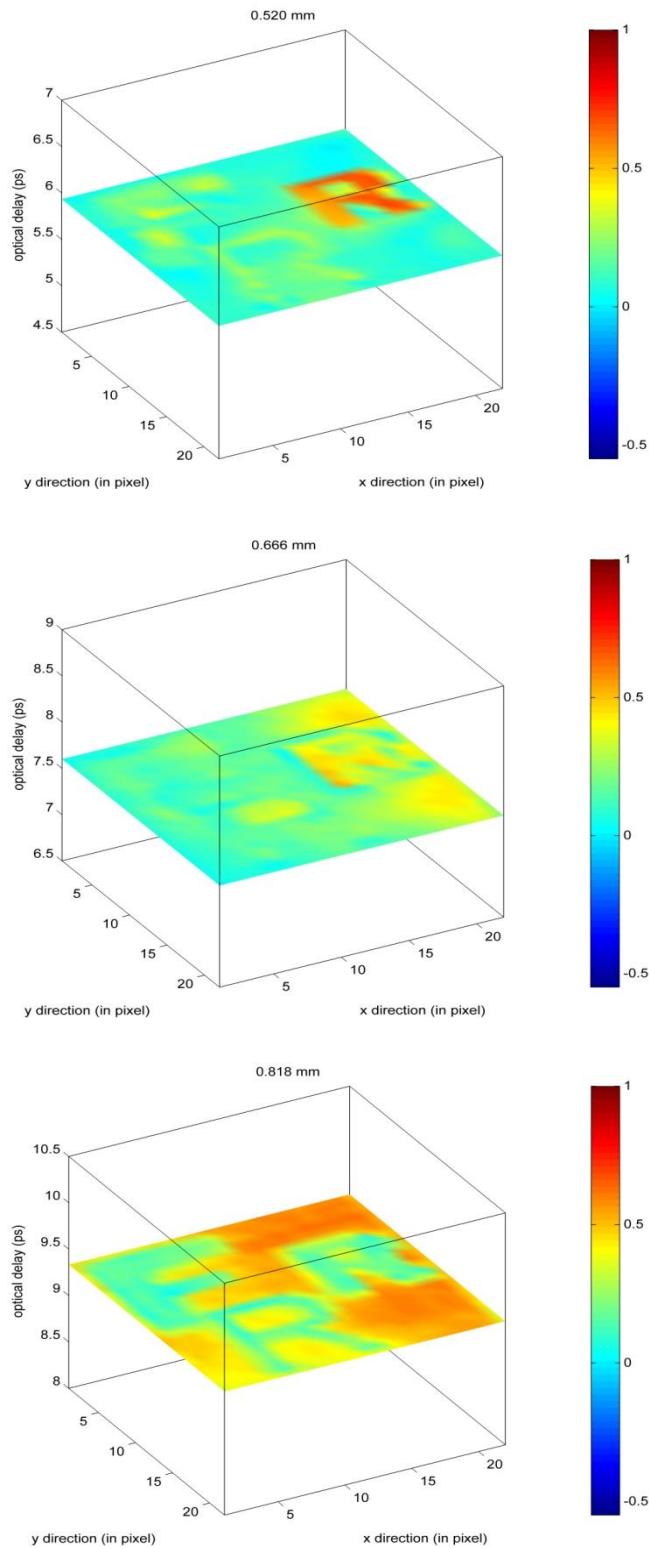
In Figures 4.4 – 4.6; while the red color shows high reflectance, the blue color shows negative value of normalized electric field amplitude reflected from layers. At 0.134 mm, higher reflectance was observed from one edge of the first letter. This letter came into view completely at 0.216 mm and higher reflection was observed from some part of the second letter at this layer. At 0.351 mm, the second letter appeared entirely and the first letter was also in sight although amplitude of reflected pulse was negative valued. Because THz pulse reflects only from the surface of aluminium, any pulse does not reflect from back side of these letters. Therefore, shapes of letters were expected to be observed at deeper cross sections than depths at which they were placed as shown in this cross section. At 0.473 mm, the third letter began to appear and it appeared completely at 0.555 mm. Image at 0.818 mm shows reflection from gold mirror on which the sample was placed.

In Figures 4.7 – 4.9, same color scale used in Figures 4.4 – 4.6 was used. Because magnitude of electric field was plotted, normalized value of data ranged from 0 to 1. However, same color scale was preferred to observe differences resulting from the use of amplitude and magnitude of reflected THz electric field. The first, second and third letters appeared at 0.123 mm, 0.216 mm and 0.473 mm inside the sample, respectively. However, higher reflectance from regions where letters were located was also observed at deeper layers than they were positioned.

Both phase and amplitude of a THz wave are modulated during its propagation through samples. While time delay (phase shift) is related to optical path length and refractive index of medium through which THz wave propagates, amplitude attenuation is associated with absorption coefficient of the medium. Therefore, the phase shift gives information about thickness and refractive index of the medium and attenuation shows opacity of the medium.

Cross sectional THz images in Figures 4.4 – 4.6 were constructed using electric field amplitude. Therefore, these images show attenuation of THz field through the sample. However, THz images in Figures 4.7 – 4.9 were constructed using electric field amplitude in combination with phase information. In consequence, phase shifts due to optical path were added to these images and clearer images of letters in depths closer to the reality were obtained.

As it can be observed from colouring of these images, reflectance values of various parts of layers are different. This indicates that edges of layers located at different depths due to presence of air gap between acetate layers.

4.2.2 TERAHERTZ IMAGING RESULTS OF SLICED TOOTH SAMPLES

Figure 4.10 and Figure 4.11 show two dimensional THz images of tooth slice presented in Figure 4.2 (a) where various sections of tooth, enamel and dentine (outer) and pulp (center), are represented. These THz images were obtained by keeping the delay axis at fixed points as that these time delays corresponded to peak THz amplitude reflected from top and bottom surfaces of a predefined pixel, respectively and scanning the sample around the THz focus. In this way, structural changes of the sample became evident.

Figure 4.10: Normalized THz electric field amplitude image of sliced tooth shown in Figure 4.2 (a) to scale at the peak of THz signal according to the reflection from top surface of tooth slice; the red color shows high reflectance.

The refractive index of enamel (3.06±0.09) is higher than dentine (2.57±0.05) in 0.5-1.5 spectral range [57]. Therefore, reflection from enamel part is expected to be

higher than dentine part. Additionally, the absorption coefficient of enamel (62 ± 7 cm^{-1}) is lower than dentine (70 ± 7 cm^{-1}) in the spectral range of 0.5-1.5 THz [57]. In consequence, THz pulse is absorbed less in enamel and reflected signal from this region is higher. The colouring of Figures 4.10 and 4.11 are consistent with these statements.
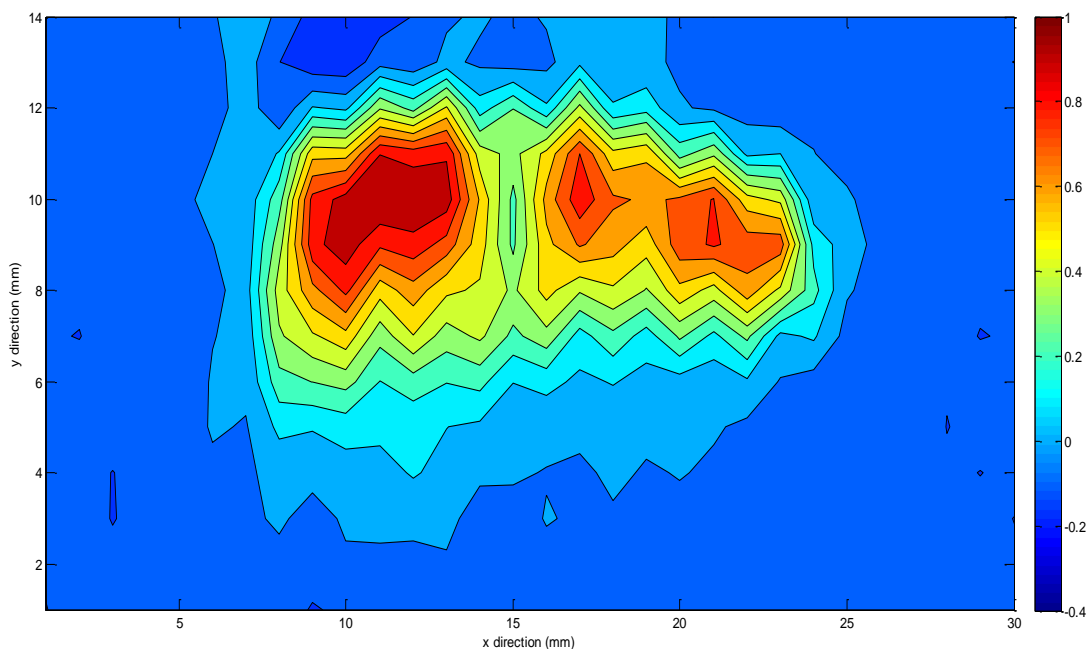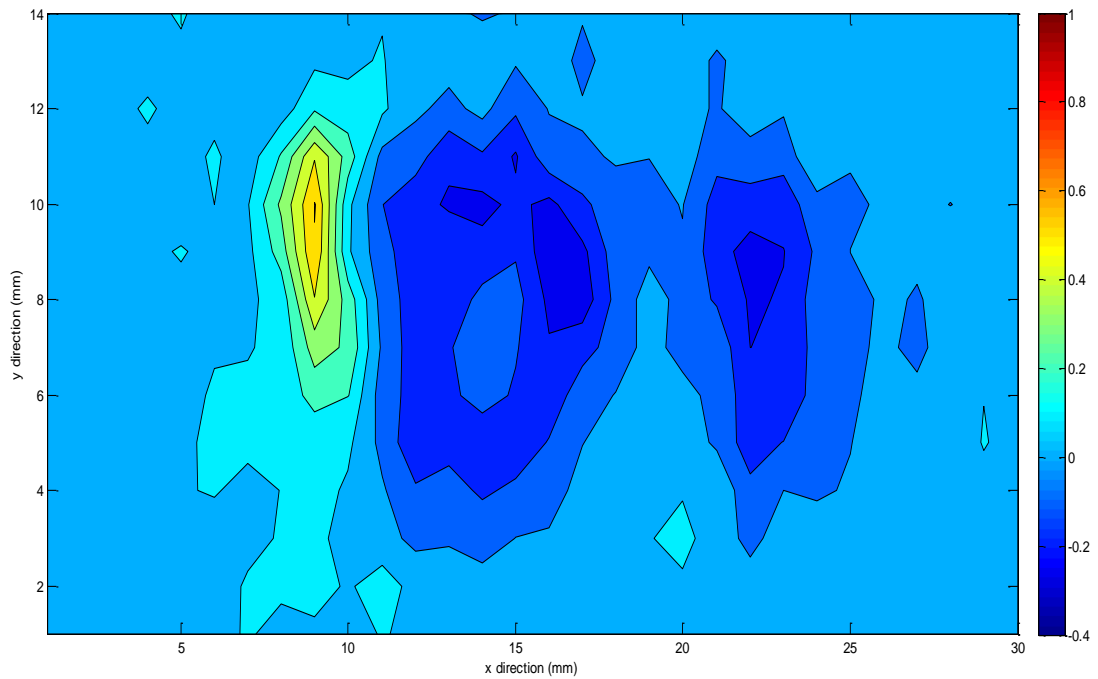

Figure 4.11: Normalized THz electric field amplitude image of sliced tooth shown in Figure 4.2 (a) to scale at the peak of THz signal according to the reflection from bottom surface of tooth slice; the red color shows high reflectance.

Normalized time domain THz waveforms measured from a healthy point and a caries point of tooth sample displayed in Figure 4.2 (b) are shown in Figure 4.12. The primary (A1) and (B1) peaks represent partial reflections from top surfaces of healthy point, A and unhealthy point, B, respectively. The secondary (A2) and (B2) peaks signify reflections from bottom surfaces of healthy point, A and caries point, B, respectively.

Reflections coming from top and bottom surfaces of tooth sample were observed as positive peaks because of the higher refractive index of tooth than air. Regions between the primary and secondary partial reflection peaks in THz waveforms from

healthy and caries points provide information about internal structures of these areas. Differences for these regions were observed in the time domain for healthy and unhealthy points.

Figure 4.12: Normalized temporal waveforms obtained from a single point THz measurement of a healthy point (A) and a caries point (B) of the tooth sample 2, respectively

Frequency domain waveforms of these healthy and caries points of same tooth sample are shown in Figure 4.13. Spectral amplitude of healthy point was extended up to 0.4 THz; however, this range was up to 0.5 THz for unhealthy point. Characteristic differences of the healthy and caries points were more precise in the frequency domain.

Measured THz waveforms in the time domain from a single point THz measurement of a healthy and an unhealthy point of tooth sample shown in Figure 4.2 (c) are displayed in Figure 4.14. Similarly, the primary (A1) and secondary (A2) peaks show

THz reflections from top and bottom surfaces of healthy point, A, respectively; while the primary (B1) and secondary (B2) peaks indicate reflections from top and bottom surfaces of unhealthy point, B, respectively.

Figure 4.13: Amplitude of reflected THz pulse from healthy (A) and caries (B) points of the tooth sample 2 in frequency domain, respectively

Although reflected amplitudes from the bottom surface of these points were weak in Figure 4.14, differences in the time domain signals were observed at delay times coming after the upper surface reflection as a result of exposure of these points to THz radiation.

Frequency domain waveforms obtained through a fast Fourier transformation of these healthy and unhealthy points for the tooth sample 3 are given in Figure 4.15. Amplitude range of the healthy point was up to 0.4 THz; however, frequencies up to 0.3 THz were observed for caries point. Healthy and unhealthy zones were likewise distinguished simply from frequency domain waveforms.
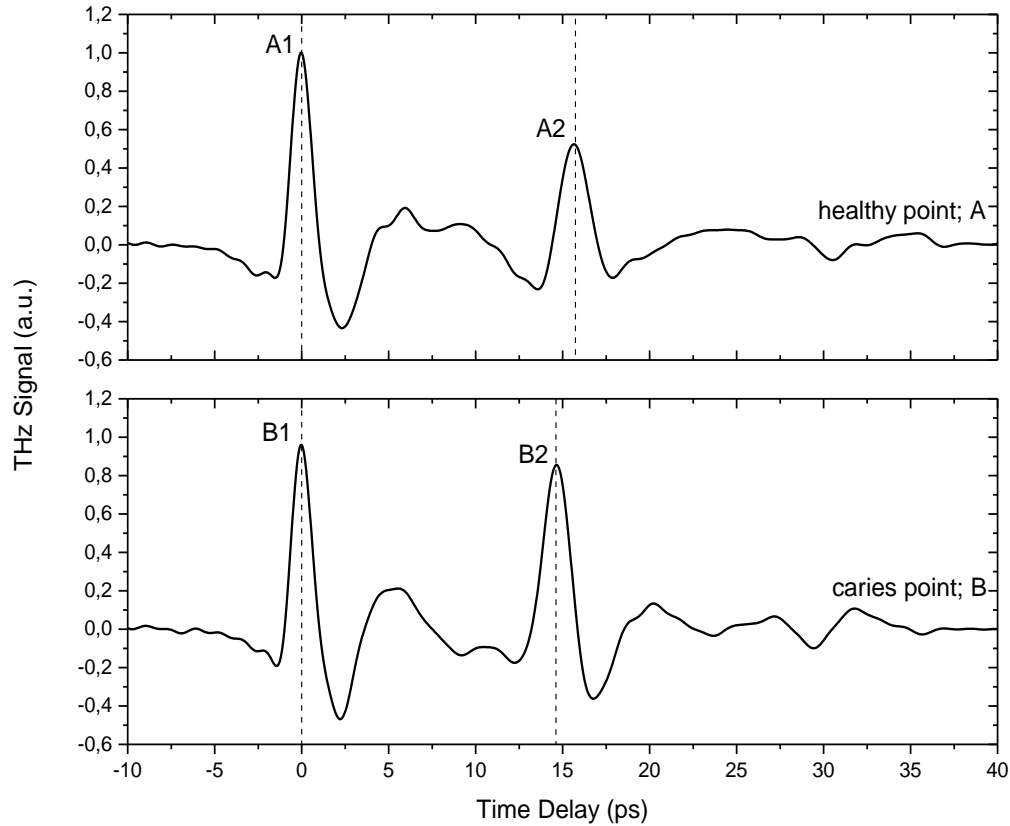
Figure 4.14: Normalized temporal waveforms obtained from a single point THz measurement of a healthy point (A) and a caries point (B) of the tooth sample 3, respectively
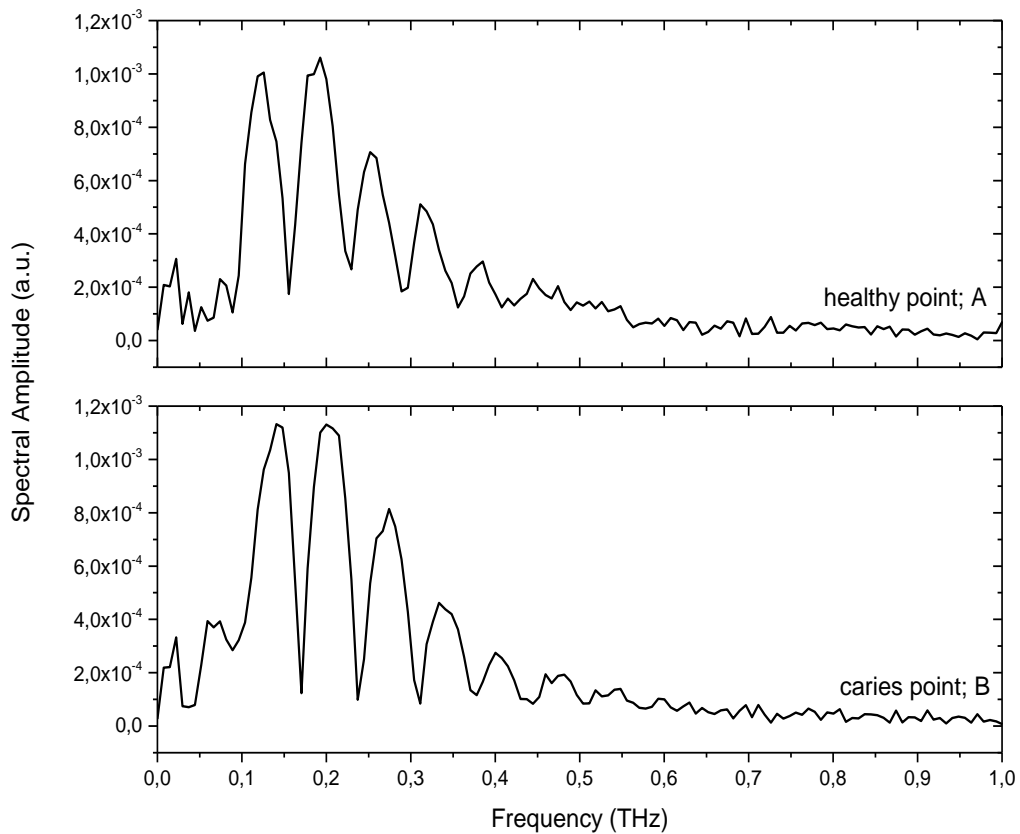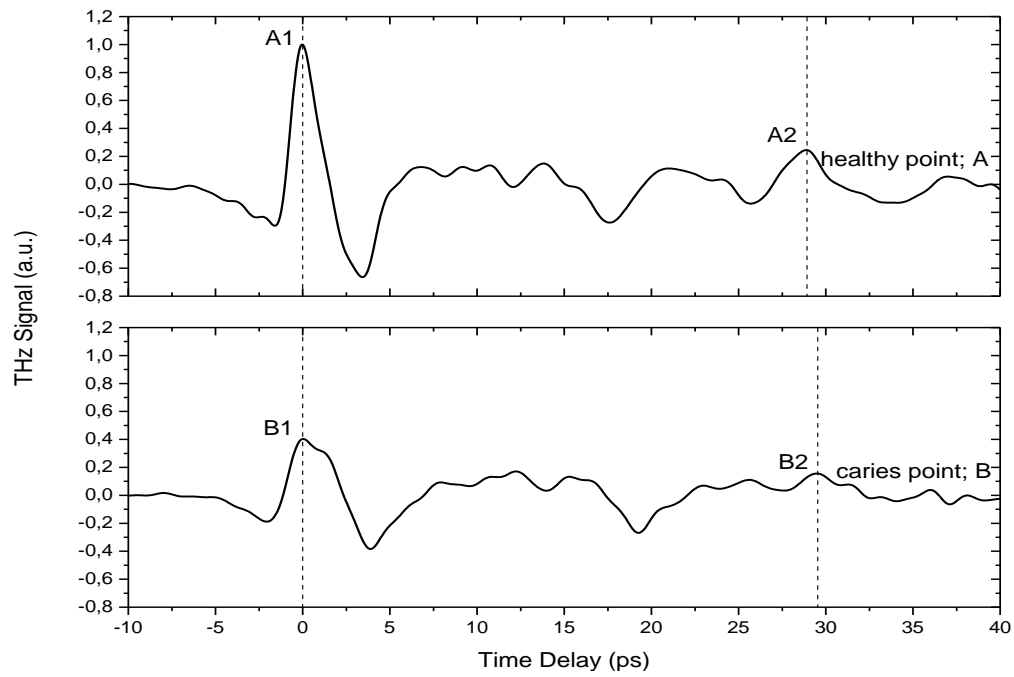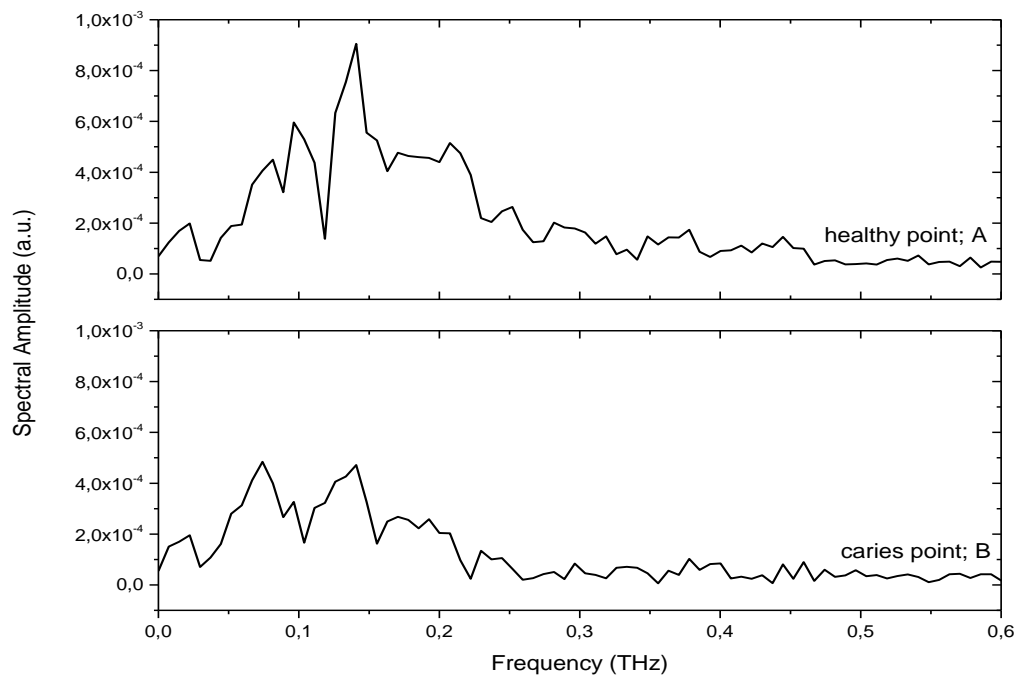

Figure 4.15: Amplitude of reflected THz pulse from healthy (A) and caries (B) points of the tooth sample 3 in frequency domain, respectively

4.3 DISCUSSION

A sample composed of metal shapes which were placed at different cross sectional depths between acetate layers was tested for non-destructive imaging of internal structure of a layered sample. Although any signal proccessing procedure has not been applied to THz data, aluminium shapes could be clearly resolved.

Dental caries, a serious prevalent disease, is the main underlying cause of tooth losses. This disease both destructs tooth structure and affects ultimately surrounding tissues and pulp. Its formation is a dynamic process in which decomposition of minerals in hard tissue is observed. Demineralization of enamel manifests the disease. While demineralization is in enamel level, the progress of demineralization can be reversed and diseased tooth can be cured with remineralization treatments [58]. However, detection of lesions is difficult at early stages due to deficiency of methods to identify precisely the presence of tooth decay on entire tooth structure [59]. Therefore, there is a requirement of new methods to monitor whole structure and characterize defects.

Transverse microradiography (TMR) is one of the methods used to investigate mineral content of lesions [60]. However, this technique requires a destructive sample preparation stage because tooth samples have to be cut into thin slices before microradiography. X-ray microtomography (XMT) is an alternative method to TMR [61]. Because this method uses ionising radiation, detrimental effects of this method on human health are significant [62, 63].

Terahertz pulsed imaging has been employed extensively in dentistry [64-66] by means of its non-destructive and non-ionizing nature. There have also been some studies on identification of natural dental caries [67] and artificial lesions [68] and detection of remineralization of artifically induced lesions [69] using TPI. These researches show the usability of TPI in studies about identification of demineralization.

Two dimensional THz images of the tooth sample 1 obtained by measuring reflected THz peak amplitude showed that differences at various parts of tooth could be

observed by TPI. Dental caries was also investigated in time and frequency domains and differences between the healthy and unhealthy regions were detected in both domains, but distinctions were more explicit in the frequency domain. These images displayed the sensitivity of THz pulse to structural changes both on surface and inside tooth samples. This potential of TPI to diagnose such changes is promising in early detection of dental caries.

Absorption coefficient of sample and signal-to-noise ratio of system determine maximum detectable penetration depth of THz radiation. Generated THz pulse in our system, however, can penetrate up to 1.5 mm depth into tooth samples. Therefore, a better SNR is required because penetration depth increases with it.

Signal-to-noise ratio together with bandwidth of the THz pulse has influence both on penetration depth and on axial resolution which determines resolving capability of a THz system. Because usable bandwidth of our system is about 0.7 THz, coherence length is then calculated as ~ 70 µm for this probe system if n=3 is used for refractive index of tooth. It is necessary to increase the bandwidth of THz pulse for resolution of smaller features. However, problems can be experienced since absorption coefficient of tooth increases with increasing frequency as a characteristic of most biological tissues.

CHAPTER 5

CONCLUSION

In this study, a THz time domain spectroscopy system operating in reflection mode was constructed for imaging in three dimensions. Three dimensional imaging of samples is achieved by scanning both the THz beam and samples around the THz focus. The system is driven by an ultrafast Er-doped mode-locked fiber laser and photoconductive antennas coupled with special collimating and focusing lenses are used for the generation and detection of the THz radiation.

In the first configuration of the THz-TDS setup, antennas used in generation and detection of THz radiation were aligned as the THz pulse was incident on samples with an angle of 30° to the normal. The beam was collimated and focused using a lens combination supplied by BATOP GmbH, Jena, Germany. However, spot diameter of THz pulse was measured as 10 mm at a focal length of 30 mm with this lens arrangement. This diameter was a limiting factor for spatial resolution. In order to improve the resolution, focusing lens of the PCA used as emitter was replaced with a biconvex F#1 25mm diameter TPX lens and measured spot diameter was about 3 mm at a focal length of 18 mm. The incident angle of THz pulse is aligned to 34° to the normal in this configuration. Bandwidth of the resultant THz pulse is up to 1 THz with a SNR of $10^4/1$.

There are some certain advantages of a THz time domain spectroscopy system in reflection mode for three dimensional imaging which are not introduced by a transmission mode system. One of these advantages is that systems using reflection mode provide for investigation of opaque and highly absorbing samples with large thicknesses. The other advantage is that reflected THz waveform includes a series of multiple pulses which represent interfaces or defects inside a material because some

portion of the terahertz pulse reflects from every refractive index change in the medium. Time delay between each reflected pulses in the resultant waveform is used to determine distances between interfaces in a sample. Therefore, measurements taken by a THz-TDS system utilizing reflection mode can be used to obtain a three dimensional image of samples where the temporal response of reflected THz waveforms gives depth profile of each sample.

The capability of the constructed THz-TDS system to distinguish inclusions inside an enclosed sample was tested using a layered sample with a total thickness of 0.6 mm. Metal shapes of thickness 80 μm were embedded inside six acetate layers of thickness 100 μm at different locations in depth. Time, position and amplitude information were collected for each pixel and thus terahertz images of cross sectional locations which are C-scan images in z- or depth direction could be obtained. Shapes of the aluminium letters could be resolved clearly in depth even though only the raw THz data was used for image reconstruction.

These measurements were sufficient to perform a time domain analysis and thus extract three dimensional image of samples in reflection mode although data analysis was more complicated than in transmission mode measurements.

Contrary to the conventional approaches in THz image construction, which use only the electric field amplitude or temporal intensity as a contrast mechanism, the approach taken here which involves the correlation between the amplitude and phase improves significantly the quality of constructed images. Because both the amplitude and phase of THz waves are modulated by the sample, adding phase information to the electric field amplitude enhanced the accuracy and quality of images.

Future work using this system will be focused on imaging biological hard tissues, such as human teeth. Tooth samples were obtained with permission with the help of Dr. Kivanc Kamburoglu at the Faculty of Dentistry of Ankara University, Ankara, Turkey. Before the analysis of three dimensional images of tooth samples, the system was used to analyze various slices of teeth in one and two dimensions. The potential of the terahertz pulsed imaging (TPI) system to diagnose structural changes in tooth samples was investigated because sensitivity of the system to such changes is a

determining factor in monitoring dental caries. Differences due to various sections of tooth were obvious in two dimensional THz images. Characteristic distinctions between healthy and caries regions of tooth slices were also observed in time and frequency domain analyses. These measurements show that THz pulsed imaging has a potential to detect dental caries at early stage of formation. However, a better SNR is essential to increase the penetration depth of THz waves into tooth samples. In addition, an increase in the bandwidth of the system can aid in the detection and help in obtaining higher spatial resolution in the obtained images.

REFERENCES

[1] Y. S. Lee. Principles of terahertz science and technology. *Springer Science+Business Media, LLC*, 2009.

[2] G. S. Park et al. Convergence of terahertz sciences in biomedical systems. *Springer Science+Business Media Dordrecht*, 2012.

[3] Ultra-broadband communication networks in the terahertz band. http://www.ece.gatech.edu/research/labs/bwn/projects/teranets/. Last accessed 28-December-2015.

[4] X. C. Zhang and J. Xu. Introduction to THz wave photonics. *Springer Science+Business Media, LLC*, 2010.

[5] S. S. Dexheimer. Terahertz spectroscopy: Principles and applications. *CRC Press*, 2008.

[6] X. C. Zhang. Terahertz wave imaging: horizons and hurdles. *Phys. Med. Biol.* 47: 3667-3677, 2002.

[7] S. W. Smye, J. M. Chamberlain, A. J. Fitzgerald, and E. Berry. The interaction between terahertz radiation and biological tissue. *Phys. Med. Biol.* 46: R101-R112, 2001.

[8] K. E. Peiponen and J. A. Zeitler. Terahertz spectroscopy and imaging. *Springer-Verlag Berlin Heidelberg*, 2013.

[9] Y. Sun et al. A promising diagnostic method: Terahertz pulsed imaging and spectroscopy. *World J. Radiol.* 3, 3: 55-65, 2011.

[10] C. A. Schmuttenmaer. Exploring dynamics in the far-infrared with terahertz spectroscopy. *Chem. Rev.* 104, 4: 1759-1780, 2004.

[11] P. U. Jepsen, D. G. Cooke, and M. Koch. Terahertz spectroscopy and imaging-Modern techniques and applications. *Laser Photonics Rev.* 5, No. 1: 124-166, 2011.

[12] J. B. Baxter and G. W. Guglietta. Terahertz spectroscopy. *Anal. Chem.* 83: 4342-4368, 2011.

[13] O. Svelto. Principles of lasers. *Plenum Press*, 1998.

[14] W. L. Chan, J. Deibel, and D. M. Mittleman. Imaging with terahertz radiation. *Rep. Prog. Phys.* 70: 1325-1379, 2007.

[15] P. R. Smith, D. H. Auston, and M. C. Nuss. Subpicosecond photoconducting dipole antennas. *IEEE J. Quantum Electron* 24, 2: 255-260, 1988.

[16] M. C. Beard, G. M. Turner, and C.A. Schmuttenmaer. Subpicosecond carrier dynamics in low-temperature grown GaAs as measured by time-resolved terahertz spectroscopy. *J. Appl. Phys.* 90: 5915-5923, 2001.

[17] A. J. Fitzgerald et al. An introduction to medical imaging with coherent terahertz frequency radiation. *Phys. Med. Biol.* 47: R67-R84, 2002.

[18] W. Zouaghi et al. Broadband terahertz spectroscopy: principles, fundamental research and potential for industrial applications. *Eur. J. Phys.* 34: S179-S199, 2013.

[19] L. Harris and P. Fowler. Absorption of gold in the far infrared. *J. Opt. Soc. Am.* 51: 164-167, 1961.

[20] K. L. F. Bane, G. Stupakov, and J. J. Tu. Reflectivity measurements for copper and aluminum in the far IR and the resistive wall impedance in the LCLS undulator. *Proceedings of EPAC*: 2955-2957, 2006.

[21] N. Karpowicz et al. Comparison between pulsed terahertz time-domain imaging and continuous wave terahertz imaging. *Semicond. Sci. Technol.* 20: S293-S299, 2005.

[22] K. Siebert et al. All-optoelectronic continuous wave THz imaging for biomedical applications. *Phys. Med. Biol.* 47, 3743, 2002.

[23] Y. Chen et al. Spectroscopic characterization of explosives in the far infrared region. *SPIE Defence and Security Symp.* #5411-2, 2004.

[24] J. Pearce and D. Mittleman. Propagation of single-cycle terahertz pulses in random media. *Opt. Lett.* 26, 2002.

[25] B. S. Ferguson et al. In vitro osteosarcoma biosensing using THz time domain spectroscopy. *Proc. SPIE-Int. Soc. Opt. Eng.* 5275, 304, 2004.

[26] Y. Watanabe et al. Component spatial pattern analysis of chemicals by use of terahertz spectroscopic imaging. *Opt. Photon. News* 14, 43, 2003.

[27] K. McClatchey, M. T. Reiten, and R. Cheville Time resolved synthetic aperture terahertz impulse imaging. *Appl. Phys. Lett.* 79: 4485-4487, 2001.

[28] B. B. Hu and M. C. Nuss. Imaging with terahertz waves. *Opt. Lett.* 20, 16: 1716-1718, 1995.

[29] D. M. Mittleman, R. H. Jacobsen, and M. C. Nuss. T-ray imaging. *IEEE Sel. Top. Quantum Electron* 2: 679-692, 1996.

[30] D. M. Mittleman, S. Hunsche, L. Boivin, and M. C. Nuss. T-ray tomography. *Opt. Lett.* 22: 904-906, 1997.

[31] J. Pearce, H. Choi, D. M. Mittleman, J. White, and D. Zimdars. T-ray reflection computed tomography. *Opt. Lett.* 30: 1653-1655 33, 2005.

[32] J. Pearce, H. Choi, D. M. Mittleman, J. White, and D. Zimdars. Terahertz wide aperture reflection tomography. *Opt. Lett.* 30: 1653-1655, 2005.

[33] E. Berry, R. D. Boyle, A. J. Fitzgerald, and J. W. Handley. Time frequency analysis in terahertz pulsed imaging. *In: Bhanu, B. and Pavlidis, I., (eds). Computer Vision: Beyond the Visible Spectrum. Advances in Pattern Recognition. Springer Verlag, London, UK.*, 2005.

[34] A. Bitzer, A. Ortner, and M. Walther. Terahertz near-field microscopy with subwavelength spatial resolution based on photoconductive antennas. *Appl. Opt.*, 49, 19: E1-E6, 2010.

[35] D. Zimdars and J. S. White. Terahertz reflection imaging for package and personnel inspection. *Proc. SPIE* 5411, *Terahertz for Military ans Security Applications II,* 78, 2004.

[36] D. Zimdars. High speed terahertz reflection imaging. *Proc. SPIE* 5692, *Advanced Biomedical and Clinical Diagnostic Systems III*, 255, 2005.

[37] Y. C. Shen. Development and application of terahertz pulsed imaging for nondesctructive inspection of pharmaceutical tablet. *IEEE Sel. Top. Quantum Electron* 14, 2: 407-415, 2008.

[38] S. Y. Huang et al. Tissue characterization using terahertz pulsed imaging in reflection geometry. *Phys. Med. Biol.* 54, 1: 149-160, 2009.

[39] E. Pickwell, B. E. Cole, A. J. Fitzgerald, M. Pepper, and V. P. Wallace. In vivo study of human skin using pulsed terahertz radiation. *Phys. Med. Biol.* 49, 9: 1595-1607, 2004.

[40] V. P. Wallace et al. Terahertz pulsed imaging of basal cell carcinoma ex vivo and in vivo. *Br. J. Dermatol.* 151, 2: 424-432, 2004.

[41] L. Ho et al. Analysis of sustained-release tablet film coats using terahertz pulsed imaging. J. Control Release 119, 3: 253-261, 2007.

[42] L. Maurer and H. Leuenberger. Terahertz pulsed imaging and near infrared imaging to monitor the coating process of pharmaceutical tablets. *Int J Pharm* 370, 1-2: 8-16, 2009.

[43] C. Stoik, M. Bohn, and J. Blackshire. Nondestructive evaluation of aircraft composites using reflective terahertz time domain spectroscopy. *Optics Express* 16, 21: 17039-17051, 2008.

[44] Y. C. Shen et al. Detection adn identification of explosives using terahertz pulsed spectroscopic imaging. *Appl. Phys. Lett.* 86, 241116, 2005.

[45] D. Crawley et al. Three-dimensional terahertz pulse imaging of dental tissue. *J. Biomed. Opt.* 8, 2: 303-307, 2003.

[46] J. A. Zeitler et al. Analysis of coating structures and interfaces in solid oral dosage forms by three dimensional terahertz pulsed imaging. *J. Pharm. Sci.* 96, 2: 330-340, 2007.

[47] P. Y. Han. A direct comparison between terahertz time-domain spectroscopy and far-infrared Fourier transform spectroscopy. *J. Appl. Phys.* 89: 2357-2359, 2011.

[48] T. I. Jeon and D. Grischkowsky. Characterization of optically dense, doped semiconductors by reflection THz time domain spectroscopy. *Appl. Phys. Lett.* 72(23): 3032-3034, 1998.

[49] A. Pashkin, M. Kempa, H. Nemec, F. Kadlec, and P. Kuzel. Phase-sensitive time-domain terahertz reflection spectroscopy. *Rev. Sci. Instrum.* 74: 4711-4717, 2003.

[50] M. V. Exter and D. Grischkowsky. Optical electrical properties of doped silicon from 0.1 to 2 THz. *Appl. Phys. Lett.* 56: 1694-1696, 1990.

[51] M. Herrmanni, M. Tani, K. Sakai, and R. Fukasawa. Terahertz imaging of silicon wafers. *J. Appl. Phys.* 91: 1247-1250, 2002.

[52] M. Khazan, R. Meissner, and I. Wilke. Convertible transmission-reflection time-domain terahertz spectrometer. *Rev. Sci. Instrum.* 72: 3427-3430, 2001.

[53] Batop. http://www.batop.de/products/terahertz/photoconductive-antenna/data-sheet/manual_PCA-40-05-10-1550.pdf. Last accessed 12-October-2015.

[54] Batop. http://www.batop.de/products/terahertz/photoconductive-antenna/data-sheet/mounts/mounted_PCA1-h.pdf. Last accessed 12-October-2015.

[55] Batop. http://www.batop.de/products/terahertz/photoconductive-antenna/data-sheet/manual_bPCA-100-05-10-1550.pdf. Last accessed 12-October-2015.

[56] Batop. http://www.batop.de/products/terahertz/THz-parts/data-sheet/FTL-f30mm.pdf. Last accessed 12-October-2015.

[57] B. E. Fitzgerald et al. Optical properties of tissue measured using terahertz pulsed imaging. *Proc. of SPIE: Medical Imaging 2003*, 459-470, 2003.

[58] D. T. Zero. Dentifrices, mouthwashes, and remineralization/caries arrestment strategies. *BMC Oral Health* 6: 1-13, 2006.

[59] S. Bala, M. Goel, S. Verma, S. Dahiya, and V. Jindal. Diagnostic modalities of early caries detection. *Indian Journal of Dental Sciences*, 3, 3, 2011.

[60] M. Huysmans and C. Longbottom. The challenges of validating diagnostic methods and selecting appropriate gold standards. *J. Dent Res.* 83, (Spec. Issue C): C48–52, 2004.

[61] S. E. P. Dowker, J. C. Elliott, G. R. Davis, and H. S. Wassif. Longitudinal study of the three-dimensional development of subsurface enamel lesions during *in vitro* demineralisation. *Caries Res.* 37: 237–245, 2003.

[62] F. Angelieri, V. Carlin, D. M. Saez, R. Pozzi, and D. A. Riberio. Mutagenicity and cytotoxicity assessment in patients undergoing orthodontic radiographs. *Dentomaxillofacial Radiology* 39: 437-440, 2010.

[63] W. T. Longstreth et al. Dental X- rays and the risk of intracranial meningioma: a population-based case-control study. *Cancer* 100(5): 1026-1034, 2004.

[64] D. A. Crawley et al. Three-dimensional terahertz pulse imaging of dental tissue. *J Biomed Opt 2003a*, 8: 303–307, 2003.

[65] K. Kamburoglu, N.Ö. Yetimoglu, and H. Altan. Characterization of primary and permanent teeth using terahertz spectroscopy. *Dentomaxillofac. Radiol.* 43, 6, 2014.

[66] Y. C. Sim, I. Maeng, and J. H. Son. Frequency-dependent characteristics of terahertz radiation on the enamel and dentin of human tooth. *Current Applied Physics 9*: 946–949, 2009.

[67] D. A. Crawley et al. Terahertz pulse imaging: a pilot study of potential applications in dentistry. *Caries Res 2003b*, 37: 352–359, 2003.

[68] E. Pickwell et al. A Comparison of Terahertz Pulsed Imaging with Transmission Microradiography for Depth Measurement of Enamel Demineralisation in vitro. *Caries Res*, 41: 49–55, 2007.

[69] D. Churchley et al. Terahertz pulsed imaging study to assess remineralization of artificial caries lesions. *Journal of Biomedical Optics*, 16(2), 2011.

APPENDIX A

TERAHERTZ IMAGES OF MULTILAYER SAMPLE THROUGH DEPTH DIRECTION

A CD which includes images of the internal of layered sample obtained by adding THz cross sectional images corresponding to depth slices of it one after another is added. The files "amplitudeimage.gif" and "magnitudeimage.gif" show false color (red color shows high reflectance) depth images toward the inside of sample obtained with normalized electric field amplitude and magnitude, reflectively.